Mon. Not. R. Astron. Soc. **368,** 253–279 (2006) doi:10.1111/j.1365-2966.2006.10105.x

Faint emission lines in the Galactic H II regions M16, M20 and NGC 3603⋆

J. García-Rojas,[1]† C. Esteban,[1] M. Peimbert,[2] M. T. Costado,[3] M. Rodríguez,[4] A. Peimbert[2] and M. T. Ruiz[5]

[1]*Instituto de Astrofísica de Canarias, E-38200 La Laguna, Tenerife, Spain*
[2]*Instituto de Astronomía, UNAM, Apdo. Postal 70-264, México 04510 D.F., Mexico*
[3]*Departamento de Astrofísica, Universidad de La Laguna, La Laguna, Spain*
[4]*Instituto Nacional de Astrofísica, Óptica y Electrónica INAOE, Apdo. Postal 51 y 216, 7200 Puebla, Puebla, Mexico*
[5]*Departamento de Astronomía, Universidad de Chile, Casilla Postal 36D, Santiago de Chile, Chile*

Accepted 2006 January 19. Received 2006 January 11; in original form 2005 November 21

ABSTRACT

We present deep echelle spectrophotometry of the Galactic H II regions M16, M20 and NGC 3603. The data have been taken with the Very Large Telescope Ultraviolet-Visual Echelle Spectrograph in the 3100–10 400 Å range. We have detected more than 200 emission lines in each region. Physical conditions have been derived using different continuum and line intensity ratios. We have derived He^+, C^{++} and O^{++} abundances from pure recombination lines as well as collisionally excited lines (CELs) for a large number of ions of different elements. We have obtained consistent estimations of the temperature fluctuation parameter, t^2, using different methods. We also report the detection of deuterium Balmer lines up to Dδ (M16) and to Dγ (M20) in the blue wings of the hydrogen lines, which excitation mechanism seems to be continuum fluorescence. The temperature fluctuation paradigm agrees with the results obtained from optical CELs, and the more uncertain ones from far-infrared fine-structure CELs in NGC 3603, although, more observations covering the same volume of the nebula are necessary to obtain solid conclusions.

Key words: ISM: abundances – H II regions – ISM: individual: M16 – ISM: individual: M20 – ISM: individual: NGC 3603.

1 INTRODUCTION

Spectrophotometric studies of Galactic H II regions provide paramount information for the study of the chemical evolution of our Galaxy. The use of echelle spectrographs at large-aperture telescopes is a step ahead in the knowledge of the physics and chemical composition of these objects. In the last years, our group and others have obtained deep intermediate and high-resolution optical spectra of bright Galactic H II regions (e.g. Peimbert, Storey & Torres-Peimbert 1993; Esteban et al. 1998, 1999a,b; Tsamis et al. 2003; Esteban et al. 2004; García-Rojas et al. 2004, 2005), and extragalactic H II regions (e.g. Esteban et al. 2002; Peimbert 2003; Tsamis et al. 2003). These observations have permitted to obtain accurate measurements of very faint recombination lines (hereafter RLs) of heavy-element ions (especially C II and O II lines), avoiding the problem of line blending. A common result of all the studies commented above is that the abundance determinations from RLs are systematically larger than those obtained using the standard methods based on the standard analysis of collisionally excited lines (hereafter CELs). The discrepancies can be of the order of a factor of 2–3. This problem may be related to the so-called temperature fluctuations suggested to be present in ionized nebulae (Torres-Peimbert, Peimbert & Daltabuit 1980). In fact, the intensity of CELs is much more strongly dependent on the temperature than RLs. This implies that RLs should be, in principle, more precise indicators of the true chemical abundances of the nebula. None the less, this is still a controversial matter that has not been solved; in fact, alternative causes have been proposed recently, such as, for example, small-scale chemical inhomogeneities (Tsamis et al. 2003; Tsamis & Péquignot 2005).

This paper presents results of Very Large Telescope (VLT) spectrophotometry obtained with the Ultraviolet-Visual Echelle Spectrograph (UVES) of three bright H II regions: M16, M20 and NGC 3603. Our data set, of an unprecedented quality, allows us to derive, with high precision, physical conditions and ionic abundances of many heavy elements and, for the first time in the three H II regions studied in this paper, C^{++} and O^{++} abundances from pure RLs.

M16 – *the Aquila nebula*, NGC 6611 – is a well-known H II region of our Galaxy. Several works about star formation in the 'elephant

⋆Based on observations collected at the European Southern Observatory, Chile, proposal number ESO 68.C-0149(A).

†E-mail: jogarcia@iac.es

trunks' have appeared in the last years, most of them related to the evaporating gaseous globules (EGGs) discovered in this object (Hester et al. 1996; McCaughrean & Andersen 2002; Thompson, Smith & Hester 2002). In particular, recent near-infrared observations have led some authors to suggest that the epoch of star formation in M16 may be near its endpoint (McCaughrean & Andersen 2002; Thompson et al. 2002). Surprisingly, there are only a few optical spectrophotometric works on the chemical composition of this object,computing the most common abundance ratios (Hawley 1978; Rodríguez 1999b; Deharveng et al. 2000).

M20 – *the Trifid nebula*, NGC 6514 – is a nearby, small and symmetrical H II region ionized by the O7 V star HD 164492A. Although many works have been carried out to understand its kinematics (e.g. Bohuski 1973a; Rosado et al. 1999) and its temperature and density structure (e.g. Bohuski 1973b; Dopita 1974; Copetti et al. 2000), there is only a handful of studies devoted to the chemical composition of this nebula. Hawley (1978) and Rodríguez (1999b) derived heavy-element abundances for M20 from spectrophotometric data. Lynds & O'Neil (1985) used long-slit spectroscopic data and narrow-band photometry to measure the intensities of several bright emission lines across the nebula, and derived He, N, O and S abundances for M20 through the computing of a dusty model. Additionally, because of the particular shape, size and dust distribution of this nebula, some works were carried out to explore the interaction between gas and dust in this region (e.g. Krishna Swamy & O'Dell 1967)

Finally, NGC 3603 is the only optically visible, giant H II region in our Galaxy (Goss & Radhakrishnan 1969; Balick, Boeshaar & Gull 1980). The study of the physical properties of this object is crucial for the knowledge of physical processes in large H II regions. Many efforts have been developed on the study of the star formation and the stellar content of NGC 3603 (e.g. Brandl et al. 1999; Stolte et al. 2004), and on the study of its kinematics (e.g. Balick et al. 1980; Clayton 1986, 1990; Nürnberger et al. 2002), but few works have studied the chemical properties of the ionized gas of this object using optical data (Melnick, Tapia & Terlevich 1989; Girardi et al. 1997; Tapia et al. 2001) and mid- and far-infrared data (Lacy, Beck & Geballe 1982; Simpson et al. 1995).

In Sections 2 and 3, we describe the observations, the data-reduction procedure and the measurement and identification of the emission lines. In Section 4, we calculate electron temperatures and densities using several diagnostic ratios and discuss the t^2 results. In Section 5, ionic abundances are determined based on both kinds of lines: CELs and RLs. Total abundances are determined in Section 6. Deuterium Balmer lines and their excitation mechanism are discussed in Section 7. The detection of velocity components in NGC 3603 is reported in Section 8. Finally, in Sections 9 and 10, we present the general discussion and the conclusions, respectively.

2 OBSERVATIONS AND DATA REDUCTION

The observations were made on 2003 March 29, 30 and 31 with UVES (D'Odorico et al. 2000), at the VLT Kueyen Telescope in Cerro Paranal Observatory (Chile). We used the standard settings in both the red and blue arms of the spectrograph, covering the spectral region from 3100 to 10 400 Å. The log of the observations is presented in Table 1.

The wavelength regions 5783–5830 and 8540–8650 Å were not observed due to a gap between the two CCDs used in the red arm. There are also five small gaps that were not observed, 9608–9612, 9761–9767, 9918–9927, 10 080–10 093 and 10 249–10 264 Å, because the five redmost orders did not fit completely within the CCD.

Table 1. Journal of observations.

Date	$\Delta\lambda$ (Å)	Exposure time (s)		
		M20	M16	NGC 3603
2003 March 29–31	3000−3900	3×600	3×900	3×600
	3800−5000	3×1800	3×1825	60, 3×1320
	4750−6800	3×600	3×900	3×600
	6700−10 400	3×1800	3×1825	60, 3×1320

The slit was oriented east–west in all the cases and the atmospheric dispersion corrector (ADC) was used to keep the same observed region within the slit, regardless of the air mass value. The slit width was set to 3 arcsec and the slit length was set to 10 arcsec in the blue arm and to 12 arcsec in the red arm; the slit width was chosen to maximize the signal-to-noise ratio (S/N) of the emission lines and to maintain the required resolution to separate most of the weak lines needed for this project. The effective resolution at a given wavelength is approximately $\Delta\lambda \sim \lambda/8800$.

The centre of the slit was placed 48 arcsec north and 40 arcsec west of BD-13 4930, for M16; 17 arcsec north and 10 arcsec east of HD164492, for M20; and 12 arcsec north and 116 arcsec east of HD 306201, for NGC 3603. All slit positions cover very bright zones of the nebulae. The final usable one-dimensional spectra were extracted from an area of 3×8.5 arcsec^2 for all the objects.

The spectra were reduced using the IRAF[1] echelle reduction package, following the standard procedure of bias subtraction, aperture extraction, flat-fielding, wavelength calibration and flux calibration. The standard stars EG 247, C-32d9927 (Hamuy et al. 1992, 1994) and HD 49798 (Turnshek et al. 1990; Bohlin & Lindler 1992) were observed for flux calibration.

3 LINE INTENSITIES AND REDDENING CORRECTION

Line intensities were measured integrating all the flux in the line between two given limits and over a local continuum estimated by eye. In the cases of line blending, a multiple Gaussian profile-fitting procedure was applied to obtain the line flux of each individual line. These measurements were made with the SPLOT routine of the IRAF package. In some cases of very tight blends or blends with very bright telluric lines, the analysis was performed via Gaussian fitting (or Voigt profiles in the case of sky emission lines) making use of the Starlink DIPSO software (Howard & Murray 1990). Also, DIPSO was used to obtain the best values for the fluxes of most of the H I Balmer lines in M20, which were affected by absorptions associated to the stellar continuum scattered light. For each single or multiple Gaussian fit, DIPSO gives the fit parameter [radial velocity centroid, Gaussian sigma, full width at half-maximum (FWHM), etc.] and their associated statistical errors.

Table 2 presents the emission-line intensities measured in the three H II regions. The first and fourth columns include the adopted laboratory wavelength, λ_0, and the observed wavelength in the heliocentric rest frame, λ_{obs}. The second and third columns include the ion and the multiplet number, or series for each line. The fifth and sixth columns list the observed flux relative to Hβ, $F(\lambda)$, and the reddening-corrected flux relative to Hβ, $I(\lambda)$. The seventh column includes the fractional error (1σ) in the line intensities. Errors were

[1] IRAF is distributed by the National Optical Astronomy Observatory, which is operated by the Association of Universities for Research in Astronomy, under cooperative agreement with National Science Foundation.

Table 2. Observed and reddening-corrected relative line fluxes $F(\lambda)$ and $I(\lambda)$, respectively, in units such that $F(\mathrm{H}\beta) = 100$.

λ_0 (Å)	Ion	Multiplet	λ_{obs} (Å)	$F(\lambda)$	$I(\lambda)^a$	Error (per cent)^b	Notes
			M 16				
3187.84	He I	3	3187.81	0.693	1.352	6	
3354.42	He I	8	3354.64	0.146	0.276	18	
3347.59	He I	7	3447.65	0.201	0.375	14	
3554.42	He I	34	3554.45	0.219	0.401	13	
3587.28	He I	32	3587.37	0.178	0.325	15	
3613.64	He I	6	3613.71	0.250	0.453	12	
3634.25	He I	28	3634.30	0.383	0.691	8	
3660.28	H I	H32	3660.41	0.112	0.200	23	
3661.22	H I	H31	3661.27	0.162	0.290	17	
3662.26	H I	H30	3662.33	0.213	0.381	13	
3663.40	H I	H29	3663.50	0.217	0.388	13	
3664.68	H I	H28	3664.73	0.210	0.376	13	
3666.10	H I	H27	3666.15	0.259	0.464	11	
3667.68	H I	H26	3667.77	0.253	0.453	12	
3669.47	H I	H25	3669.57	0.322	0.575	10	
3671.48	H I	H24	3671.56	0.362	0.646	9	
3673.76	H I	H23	3673.86	0.398	0.710	8	
3676.37	H I	H22	3676.44	0.398	0.711	8	
3679.36	H I	H21	3679.43	0.434	0.774	8	
3682.81	H I	H20	3682.89	0.434	0.772	8	
3686.83	H I	H19	3686.91	0.565	1.005	7	
3691.56	H I	H18	3691.62	0.594	1.054	6	
3697.15	H I	H17	3697.24	0.684	1.213	6	
3703.86	H I	H16	3703.94	0.804	1.423	5	
3705.04	He I	25	3705.10	0.378	0.669	9	
3711.97	H I	H15	3712.05	0.972	1.715	5	
3721.94	[S III]	2F	3721.96	1.679	2.955	4	
3721.94	H I	H14					
3726.03	[O II]	1F	3726.16	88.191	154.979	4	
3728.82	[O II]	1F	3728.91	69.245	121.581	4	
3734.37	H I	H13	3734.46	1.580	2.770	4	
3750.15	H I	H12	3750.24	2.014	3.511	4	
3770.63	H I	H11	3770.72	2.503	4.336	4	
3797.90	H I	H10	3797.98	3.424	5.874	4	
3819.61	He I	22	3819.70	0.653	1.112	6	
3835.39	H I	H9	3835.47	4.845	8.197	4	
3856.02	Si II	1	3856.07	0.126	0.211	10	
3856.12	O II	12					
3862.59	Si II	1	3862.59	0.080	0.133	14	
3867.48	He I	20	3867.54	0.077	0.129	14	
3868.75	[Ne III]	1F	3868.81	2.162	3.612	4	
3871.82	He I	60	3871.82	0.065	0.109	16	
3888.65	He I	2	3889.00	11.284	18.687	3	
3889.05	H I	H8					
3918.98	C II	4	3918.92	0.084	0.138	13	
3920.68	C II	4	3920.73	0.099	0.162	12	
3926.53	He I	58	3926.64	0.087	0.141	13	
3964.73	He I	5	3964.81	0.530	0.849	4	
3967.46	[Ne III]	1F	3967.52	0.681	1.090	4	
3970.07	H I	H7	3970.15	10.591	16.928	3	
4009.22	He I	55	4009.30	0.132	0.207	9	
4026.08	N II	40	4026.28	1.276	1.987	3	
4026.21	He I	18					
4068.60	[S II]	1F	4068.72	2.264	3.452	3	
4076.35	[S II]	1F	4076.47	0.898	1.364	4	
4100.62	D I	D6	4100.76	0.015	0.022	:	
4101.74	H I	H6	4101.82	17.800	26.689	3	
4120.82	He I	16	4120.99	0.125	0.186	10	
4143.76	He I	53	4143.86	0.217	0.318	6	
4267.15	C II	6	4267.23	0.198	0.272	7	

Table 2 – *continued*

λ_0 (Å)	Ion	Multiplet	λ_{obs} (Å)	$F(\lambda)$	$I(\lambda)$[a]	Error (per cent)[b]	Notes
4303.61	O II	65a	4303.88	0.043	0.058	23	
4303.82	O II	53a					
4319.63	O II	2	4319.75	0.012	0.016	:	
4326.40	O I		4326.50	0.024	0.031	:	
4339.29	D I	D5	4339.44	0.022	0.030	38	
4340.47	H I	H5	4340.55	35.834	47.277	3	
4345.55	O II	65c	4345.54	0.029	0.038	32	
4345.56	O II	2					
4363.21	[O III]	2F	4363.26	0.147	0.192	8	
4368.25	O I	5	4368.58	0.094	0.122	12	
4387.93	He I	51	4388.01	0.382	0.491	4	
4437.55	He I	50	4437.60	0.040	0.050	24	
4471.48	He I	14	4471.59	3.240	3.977	3	
4562.60	Mg I]	1	4562.79	0.030	0.035	31	
4571.10	Mg I]	1	4571.37	0.066	0.076	16	
4607.06	[Fe III]	3F	4607.21	0.021	0.024	:	
4607.16	N II	5					
4621.39	N II	5	4621.42	0.035	0.039	28	
4630.54	N II	5	4630.61	0.046	0.052	22	
4638.86	O II	1	4638.90	0.036	0.040	26	
4641.81	O II	1	4641.83	0.031	0.034	29	
4643.06	N II	5	4643.17	0.028	0.031	33	
4649.13	O II	1	4649.24	0.051	0.056	20	
4650.84	O II	1	4650.94	0.045	0.050	22	
4658.10	[Fe III]	1F	4658.25	0.138	0.153	9	
4661.63	O II	1	4661.54	0.034	0.038	27	
4701.53	[Fe III]	3F	4701.73	0.038	0.041	26	
4711.37	[Ar IV]	1F	4711.42	0.020	0.021	:	
4713.14	He I	12	4713.27	0.351	0.379	4	
4733.91	[Fe III]	3F	4733.92	0.025	0.026	37	*e*
4754.69	[Fe III]	3F	4754.88	0.024	0.026	37	
4769.43	[Fe III]	3F	4769.63	0.017	0.018	:	
4814.55	[Fe II]	2F	4814.77	0.017	0.018	:	
4815.51	S II	9	4815.65	0.018	0.018	:	*g*
4860.03	D I	D4	4860.19	0.032	0.032	29	
4861.33	H I	H4	4861.43	100.000	100.000	3	
4881.00	[Fe III]	2F	4881.20	0.059	0.059	22	
4921.93	He I	48	4922.03	1.091	1.058	3	
4958.91	[O III]	1F	4958.99	29.222	27.824	3	
5006.84	[O III]	1F	5006.93	88.392	82.269	3	
5015.68	He I	4	5015.79	2.228	2.065	3	
5032.43	S II	7	5032.47	0.063	0.058	37	*g*
5041.03	Si II	5	5041.10	0.064	0.059	36	
5047.74	He I	47	5047.90	0.231	0.211	12	
5055.98	Si II	5	5056.13	0.164	0.149	16	
5056.31	Si II	5					
5158.78	[Fe II]	19F	5159.08	0.045	0.039	:	
5197.90	[N I]	1F	5198.18	0.519	0.443	6	
5200.26	[N I]	1F	5200.53	0.367	0.313	8	
5270.40	[Fe III]	1F	5270.71	0.088	0.073	27	
5517.71	[Cl III]	1F	5517.81	0.541	0.403	6	
5537.88	[Cl III]	1F	5537.98	0.475	0.351	7	
5545.00	N I	29	5545.25	0.046	0.034	:	
5545.15	N I	29					
5577.34	[O I]	3F	5577.89	16.156	11.692	3	
5666.64	N II	3	5666.68	0.042	0.029	:	
5679.56	N II	3	5679.81	0.043	0.030	:	
5686.21	N II	3	5686.18	0.041	0.028	:	*c*
5710.76	N II	3	5710.88	0.022	0.015	:	
5754.64	[N II]	3F	5754.78	2.110	1.403	4	
5875.64	He I	11	5875.78	18.461	11.636	3	
5978.83	Si II	4	5979.09	0.078	0.047	:	

Table 2 – *continued*

λ_0 (Å)	Ion	Multiplet	λ_{obs} (Å)	$F(\lambda)$	$I(\lambda)^a$	Error (per cent)^b	Notes
6046.44	O I	22	6046.71	0.052	0.030	:	
6300.30	[O I]	1F	6300.73	7.954	4.213	4	
6312.10	[S III]	3F	6312.24	1.941	1.024	4	
6347.11	Si II	2	6347.29	0.184	0.095	15	
6363.78	[O I]	1F	6364.20	2.678	1.384	4	
6371.36	Si II	2	6371.52	0.098	0.051	25	
6461.95	C II	17.04	6461.84	0.065	0.032	36	
6462.13	C II	17.04					
6548.03	[N II]	1F	6548.27	104.213	50.143	4	
6561.04	D I	D3	6561.31	0.063	0.030	27	
6562.82	H I	H3	6562.96	614.888	294.183	4	
6578.05	C II	2	6578.11	0.653	0.310	6	
6583.41	[N II]	1F	6583.64	326.951	155.179	4	
6678.15	He I	46	6678.30	7.113	3.255	4	
6716.47	[S II]	2F	6716.68	51.101	23.038	4	
6730.85	[S II]	2F	6731.06	65.429	29.334	4	
7002.23	O I	21	7002.58	0.195	0.079	8	*c*
7065.28	He I	10	7065.41	5.574	2.195	5	
7111.47	C I	^{3}D–^{3}F^0	7111.74	0.015	0.006	:	
7113.18	C I	^{3}D–^{3}F^0	7113.51	0.012	0.005	:	
7115.17	C I	^{3}D–^{3}F^0	7115.52	0.013	0.005	:	
7116.99	C I	^{3}D–^{3}P^0	7117.36	0.014	0.005	:	*g*
7135.78	[Ar III]	1F	7135.94	24.107	9.235	5	
7155.14	[Fe II]	14F	7155.42	0.087	0.033	14	
7231.12	C II	3	7231.45	0.261	0.096	7	
7236.19	C II	3	7236.63	0.483	0.178	6	
7254.38	O I	20	7254.80	0.125	0.046	11	
7281.35	He I	45	7281.54	1.535	0.556	5	
7298.05	He I	1/9	7298.17	0.061	0.022	18	
7318.39	[O II]	2F	7319.25	2.228	0.795	5	
7319.99	[O II]	2F	7320.35	7.705	2.747	5	
7329.66	[O II]	2F	7329.90	4.777	1.697	5	
7330.73	[O II]	2F	7330.99	4.099	1.455	5	
7377.83	[Ni II]	2F	7378.19	0.108	0.038	12	
7423.64	N I	3	7423.98	0.045	0.016	23	
7442.30	N I	3	7442.66	0.082	0.028	14	
7452.54	[Fe II]	14F	7452.76	0.039	0.013	25	
7468.31	N I	3	7468.65	0.114	0.039	11	
7499.85	He I	1/8	7500.08	0.098	0.032	13	
7751.10	[Ar III]	2F	7751.33	8.864	2.677	6	
7771.94	O I	1	7772.08	0.087	0.026	23	*c*
7782.18	Mn I		7782.55	0.032	0.009	31	*g*
7801.79	V I		7802.18	0.018	0.005	:	*g*
7816.13	He I	1/7	7816.29	0.212	0.063	9	
7837.85	[Co I]		7838.10	0.044	0.013	24	
7862.85	Fe II]		7862.93	0.019	0.006	:	*g*
7875.99	[P II]	^{1}D–^{1}S	7876.20	0.031	0.009	31	
7959.70	N I		7960.11	0.054	0.015	20	*g*
8116.	He I	4/16	8116.62	0.027	0.007	35	
8150.57	Si I	20	8151.08	0.018	0.004	:	
8184.85	N I	2	8185.21	0.057	0.015	19	
8188.01	N I	2	8188.40	0.121	0.031	12	
8216.28	N I	2	8216.68	0.149	0.038	11	
8223.14	N I	2	8223.51	0.156	0.040	10	
8245.64	H I	P42	8245.82	0.128	0.032	11	
8247.73	H I	P41	8248.00	0.168	0.043	10	*c*
8249.97	H I	P40	8250.20	0.134	0.034	11	
8252.40	H I	P39	8252.62	0.175	0.044	10	
8255.02	H I	P38	8255.28	0.207	0.052	9	
8257.85	H I	P37	8258.12	0.161	0.041	10	
8260.93	H I	P36	8261.21	0.201	0.051	9	
8264.28	H I	P35	8264.58	0.224	0.056	9	

Table 2 – *continued*

λ_0 (Å)	Ion	Multiplet	λ_{obs} (Å)	$F(\lambda)$	$I(\lambda)^a$	Error (per cent)^b	Notes
8267.94	H I	P34	8268.15	0.221	0.055	9	
8271.93	H I	P33	8272.11	0.240	0.060	9	
8276.31	H I	P32	8276.53	0.276	0.069	8	
8281.12	H I	P31	8281.69	0.241	0.060	9	
8286.43	H I	P30	8286.60	0.275	0.069	8	
8292.31	H I	P29	8292.52	0.339	0.085	8	
8298.83	H I	P28	8299.03	0.467	0.116	8	*c*
8306.11	H I	P27	8306.37	0.346	0.086	8	
8314.26	H I	P26	8314.48	0.468	0.116	8	
8323.42	H I	P25	8323.64	0.534	0.132	8	
8333.78	H I	P24	8333.97	0.571	0.140	8	
8334.75	Fe II]		8335.07	0.105	0.026	14	*g*
8343.33	He I	4/12	8342.56	0.059	0.014	19	
8359.00	H I	P22	8359.22	0.725	0.177	7	
8361.67	He I	1/6	8361.88	0.351	0.085	8	
8374.48	H I	P21	8374.69	0.761	0.184	7	
8392.40	H I	P20	8392.59	0.943	0.227	7	
8387.77	Fe I		8388.04	0.040	0.010	25	*g*
8413.32	H I	P19	8413.54	1.001	0.240	7	
8437.96	H I	P18	8438.17	1.192	0.283	7	
8444.34	He I	4/11	8444.68	0.060	0.014	19	
8446.25	O I	4	8446.87	2.034	0.482	7	*c*
8446.36	O I	4					
8446.76	O I	4					
8459.32	[Cr II]		8459.68	0.074	0.018	16	*g*
8467.25	H I	P17	8467.49	1.350	0.318	7	
8486.27	He I	6/16	8486.46	0.073	0.017	16	
8502.48	H I	P16	8502.71	1.758	0.410	7	
8518.04	He I	2/8	8518.24	0.021	0.004	:	
8528.99	He I	6/15	8529.24	0.041	0.009	25	
8665.02	H I	P13	8665.14	4.074	0.906	8	*c*
8680.28	N I	1	8680.95	0.493	0.109	8	
8683.40	N I	1	8683.79	0.111	0.024	13	
8686.15	N I	1	8686.70	0.292	0.064	9	
8703.25	N I	1	8703.59	0.077	0.017	16	
8711.70	N I	1	8712.07	0.084	0.019	15	
8718.84	N I	1	8719.31	0.048	0.011	22	
8727.13	[C I]	3F	8727.50	0.815	0.178	8	
8733.43	He I	6/12	8733.65	0.134	0.029	12	
8750.47	H I	P12	8750.70	4.260	0.925	8	
8848.05	He I	7/11	8848.15	0.069	0.015	17	
8862.79	H I	P11	8863.02	5.846	1.235	8	*c*
8889.00	C II]		8889.42	0.054	0.011	21	*g*
8893.87	V I]		8894.23	0.078	0.016	16	*g*
8946.05	Fe II]		8946.44	0.043	0.009	:	*g*
8996.99	He I	6/10	8997.18	0.233	0.048	10	
9014.91	H I	P10	9015.15	7.737	1.578	8	
9019.19	Fe I		9019.63	0.078	0.016	16	*g*
9029.30	C II		9029.47	0.114	0.023	13	*g*
9068.90	[S III]	1F	9069.16	121.058	24.419	8	
9094.83	C I	3	9095.26	0.199	0.040	10	
9111.81	C I	3	9112.22	0.073	0.015	17	
9113.70	Cl II]		9114.04	0.038	0.008	:	*g*
9123.60	[Cl II]	1F	9123.95	0.479	0.095	9	
9210.28	He I	6/9	9210.55	0.347	0.068	9	
9229.01	H I	P9	9229.26	11.076	2.161	8	
9405.73	C I	$^1P^0$–^1D	9406.11	0.127	0.024	12	*g*
9463.57	He I	1/5	9463.84	0.302	0.056	9	
9516.57	He I	4/7	9516.70	0.262	0.048	10	
9526.16	He I	6/8	9526.55	0.386	0.071	9	
9530.60	[S III]	1F	9531.21	321.963	59.257	8	

Table 2 – *continued*

λ_0 (Å)	Ion	Multiplet	λ_{obs} (Å)	$F(\lambda)$	$I(\lambda)^a$	Error (per cent)^b	Notes
9545.97	H I	P8	9546.21	13.877	2.547	8	*d*
9702.62	He I	75	9703.34	0.086	0.015	16	*d*
9824.13	[C I]	1F	9824.53	1.618	0.283	9	
9850.26	[C I]	1F	9850.66	5.069	0.882	9	
9903.46	C II	17.02	9903.55	0.214	0.037	13	*d*
9903.88	C II	17.02					
10 027.70	He I	6/7	10 027.91	0.878	0.148	9	
10 049.37	H I	P7	10 049.64	30.179	5.080	9	
10 320.49	[S II]	3F	10 320.77	4.780	0.771	9	
10 336.41	[S II]	3F	10 336.66	4.039	0.650	9	
10 370.50	[S II]	3F	10 370.79	2.109	0.338	9	
			M 20				
3187.84	He I	3	3187.72	2.364	3.375	5	
3354.42	He I	8	3354.54	0.177	0.239	21	
3447.59	He I	7	3447.54	0.280	0.370	15	
3478.97	He I	48	3479.09	0.087	0.115	35	
3487.73	He I	42	3487.76	0.064	0.083	:	
3498.66	He I	40	3498.61	0.061	0.079	:	
3512.52	He I	38	3512.49	0.172	0.224	21	
3530.50	He I	36	3530.48	0.125	0.162	27	
3554.42	He I	34	3554.40	0.212	0.274	18	
3587.28	He I	32	3587.25	0.271	0.346	15	
3613.64	He I	6	3613.61	0.316	0.401	13	
3634.25	He I	28	3634.21	0.300	0.379	14	
3656.10	H I	H38	3656.13	0.123	0.154	27	
3656.67	H I	H37	3656.72	0.100	0.126	32	
3657.27	H I	H36	3657.20	0.077	0.097	39	
3656.11	H I	H35	3657.86	0.169	0.212	21	
3658.64	H I	H34	3658.59	0.189	0.237	20	
3659.42	H I	H33	3659.32	0.256	0.321	16	
3660.28	H I	H32	3660.32	0.161	0.202	22	
3661.22	H I	H31	3661.18	0.348	0.436	12	
3662.26	H I	H30	3662.23	0.345	0.433	12	
3663.40	H I	H29	3663.35	0.510	0.639	9	
3664.68	H I	H28	3664.61	0.236	0.296	17	
3666.10	H I	H27	3666.04	0.314	0.394	13	
3667.68	H I	H26	3667.62	0.277	0.347	15	
3669.47	H I	H25	3669.40	0.309	0.387	14	
3671.48	H I	H24	3671.41	0.470	0.589	10	
3673.76	H I	H23	3673.70	0.507	0.634	10	
3676.37	H I	H22	3676.30	0.557	0.696	9	
3679.36	H I	H21	3679.30	0.616	0.770	8	
3682.81	H I	H20	3682.76	0.643	0.804	8	
3686.83	H I	H19	3686.77	0.771	0.963	7	
3691.56	H I	H18	3691.50	0.812	1.012	7	
3697.15	H I	H17	3697.10	1.002	1.247	6	
3703.86	H I	H16	3703.80	1.197	1.485	6	
3705.04	HeI	25	3704.98	0.340	0.422	13	
3711.97	H I	H15	3711.92	1.353	1.677	5	
3721.83	[S III]	2F	3721.68	0.914	1.130	6	
3721.94	H I	H1	3721.92	1.388	1.717	5	
3726.03	[O II]	1F	3725.97	118.617	146.604	3	
3728.82	[O II]	1F	3728.73	140.298	173.307	3	
3734.37	H I	H13	3734.32	2.183	2.694	4	
3750.15	H I	H12	3750.10	2.797	3.441	4	
3770.63	H I	H11	3770.58	3.483	4.268	4	
3797.90	H I	H10	3797.85	4.609	5.619	4	
3819.61	He I	20	3819.58	0.806	0.979	6	
3835.39	H I	H9	3835.33	6.339	7.674	3	
3856.02	Si II	1	3855.99	0.091	0.110	26	
3856.13	O II	12					
3867.48	He I	20	3867.47	0.058	0.070	26	
3868.75	[Ne III]	1F	3868.78	1.095	1.318	6	

Table 2 – *continued*

λ_0 (Å)	Ion	Multiplet	λ_{obs} (Å)	$F(\lambda)$	$I(\lambda)^a$	Error (per cent)^b	Notes
3871.60	He I	60	3871.72	0.082	0.099	19	
3888.65	He I	2	3888.59	5.536	6.639	3	
3867.48	He I	20	3867.47	0.058	0.070	26	
3868.75	[Ne III]	1F	3868.78	1.095	1.318	6	
3889.05	H I	H8	3888.98	10.288	12.338	3	
3918.98	C II	4	3918.86	0.079	0.094	20	
3920.68	C II	4	3920.66	0.118	0.141	14	
3926.53	He I	58	3926.51	0.105	0.125	16	
3964.73	He I	5	3964.69	0.679	0.803	4	
3967.46	[Ne III]	1F	3967.49	0.360	0.425	6	
3970.07	H I	H7	3970.01	13.845	16.371	3	
4009.22	He I	55	4009.20	0.140	0.165	12	
4023.98	He I	54	4023.94	0.023	0.026	:	
4026.08	N II	40	4026.16	1.533	1.794	3	
4026.21	He I	18					
4068.60	[S II]	1F	4068.50	1.553	1.802	3	
4076.35	[S II]	1F	4076.25	0.542	0.627	5	
4101.74	H I	H6	4101.67	22.203	25.601	3	
4120.82	He I	16	4120.78	0.061	0.071	25	
4143.76	He I	53	4143.71	0.176	0.201	10	
4153.30	O II	19	4153.34	0.030	0.034	:	
4168.97	He I	52	4168.92	0.039	0.044	37	
4169.22	O II	19					
4201.35	N II	49	4201.29	0.056	0.063	27	
4243.97	[Fe II]	21F	4243.90	0.037	0.041	:	
4247.22	N II		4247.14	0.026	0.029	:	*g*
4267.15	C II	6	4267.15	0.151	0.170	12	
4287.40	[Fe II]	7F	4287.30	0.066	0.074	24	
4339.29	D I	D5	4339.11	0.020	0.022	:	
4340.47	H I	H5	4340.40	42.225	46.999	3	
4345.55	O II	65c	4345.52	0.032	0.036	:	
4345.56	O II	2					
4359.34	[Fe II]	7F	4359.26	0.057	0.063	27	
4363.21	[O III]	2F	4363.20	0.134	0.148	13	
4368.15	O I	5	4368.11	0.025	0.027	:	
4368.25	O I	5					
4387.93	He I	51	4387.89	0.387	0.426	6	
4413.78	[Fe II]	7F	4413.69	0.036	0.039	:	
4437.55	He I	50	4437.50	0.061	0.066	25	
4452.10	[Fe II]	7F	4451.91	0.041	0.045	36	
4452.37	O II	5					
4471.48	He I	14	4471.45	3.309	3.584	3	
4562.60	Mg I]	1	4562.51	0.030	0.032	:	
4571.10	Mg I]	1	4570.96	0.012	0.013	:	
4630.54	N II	5	4630.46	0.026	0.027	:	
4641.81	O II	1	4641.83	0.029	0.030	:	
4643.06	N II	5	4643.05	0.029	0.030	:	
4649.13	O II	1	4649.18	0.035	0.036	:	
4650.84	O II	1	4650.93	0.016	0.017	:	
4658.10	[Fe III]	3F	4658.05	0.227	0.236	8	
4661.63	O II	1	4661.71	0.017	0.018	:	
4701.62	[Fe III]	3F	4701.50	0.050	0.051	30	
4711.37	[Ar IV]	1F	4711.50	0.030	0.031	:	
4713.14	He I	12	4713.12	0.306	0.315	6	
4754.83	[Fe III]	3F	4754.69	0.028	0.029	:	
4788.13	N II	20	4788.21	0.027	0.027	:	
4814.55	[Fe II]	20F	4814.42	0.017	0.018	:	
4815.51	S II	9	4815.51	0.021	0.021	:	
4860.03	D I	D4	4859.78	0.039	0.039	38	
4861.33	H I	H4	4861.25	100.000	100.000	3	
4881.00	[Fe III]	2F	4880.96	0.062	0.062	25	

Table 2 – *continued*

λ_0 (Å)	Ion	Multiplet	λ_{obs} (Å)	$F(\lambda)$	$I(\lambda)^a$	Error (per cent)^b	Notes
4921.93	He I	48	4921.88	1.007	1.000	3	
4924.50	[Fe III]	2F	4924.60	0.017	0.017	:	
4958.91	[O III]	1F	4958.95	19.374	19.006	3	
4985.90	[Fe III]	2F	4985.80	0.114	0.111	14	
4994.37	N II	94	4994.45	0.019	0.018	:	*g*
5006.84	[O III]	1F	5006.88	60.621	58.931	3	
5011.30	[Fe III]	1F	5011.17	0.037	0.036	35	
5015.68	He I	4	5015.64	2.040	1.979	3	
5041.03	Si II	5	5040.97	0.038	0.037	34	
5047.74	He I	47	5047.71	0.160	0.155	11	
5055.98	Si II	5	5055.91	0.065	0.063	22	
5056.31	Si II	5					
5191.82	[Ar III]	1F	5191.58	0.050	0.047	27	
5197.90	[N I]	1F	5197.76	0.301	0.283	7	
5200.26	[N I]	1F	5200.13	0.264	0.249	7	
5261.61	[Fe II]	19F	5261.30	0.048	0.045	28	
5270.30	[Fe III]	1F	5270.46	0.116	0.107	14	
5273.38	[Fe II]	18F	5273.18	0.022	0.020	:	
5517.71	[Cl III]	1F	5517.62	0.474	0.422	5	
5537.88	[Cl III]	1F	5537.76	0.352	0.313	6	
5666.64	N II	3	5666.60	0.027	0.023	:	
5754.64	[N II]	3F	5754.48	1.130	0.965	4	
5875.64	He I	11	5875.61	12.312	10.293	3	
5978.83	Si II	4	5978.83	0.055	0.045	25	
6046.44	O I	22	6046.20	0.021	0.017	:	
6300.30	[O I]	1F	6300.11	1.262	0.997	4	
6312.10	[S III]	3F	6311.99	1.193	0.941	4	
6347.11	Si II	2	6347.03	0.075	0.059	20	
6363.78	[O I]	1F	6363.58	0.430	0.337	6	
6371.36	Si II	2	6371.29	0.049	0.038	28	
6461.95	C II	17.04	6461.75	0.055	0.043	25	*e*
6462.13	C II	17.04					
6548.03	[N II]	1F	6547.93	47.276	36.228	4	
6561.04	D I	D3	6560.68	0.073	0.056	21	
6562.82	H I	H3	6562.71	374.754	286.694	4	
6578.05	C II	2	6578.01	0.466	0.356	6	
6583.41	[N II]	1F	6583.31	145.329	110.921	4	
6678.15	He I	46	6678.11	3.949	2.983	4	
6716.47	[S II]	2F	6716.30	32.072	24.131	4	
6730.85	[S II]	2F	6730.68	28.338	21.290	4	
7002.23	O I	21	7001.89	0.051	0.037	16	
7065.28	He I	10	7065.15	2.424	1.765	4	
7105.42	Si I		7105.24	0.015	0.011	:	*g*
7111.47	C I	^3D–$^3F^0$	7111.18	0.022	0.016	33	
7135.78	[Ar III]	1F	7135.72	12.401	8.971	4	
7155.14	[Fe II]	14F	7154.98	0.028	0.020	27	
7160.58	He I	1/10	7160.39	0.030	0.022	25	
7231.34	C II	3	7231.30	0.104	0.075	9	
7236.19	C II	3	7236.41	0.176	0.126	7	
7281.35	He I	45	7281.26	0.730	0.522	5	
7298.05	He I	1/9	7298.00	0.040	0.029	20	
7318.39	[O II]	2F	7318.88	0.763	0.543	5	
7319.99	[O II]	2F	7319.97	2.634	1.876	4	
7329.66	[O II]	2F	7329.61	1.882	1.339	4	
7330.73	[O II]	2F	7330.61	1.411	1.004	4	
7377.83	[Ni II]	2F	7377.69	0.046	0.032	18	
7423.64	N I	3	7423.47	0.027	0.019	29	*c*
7442.30	N I	3	7442.03	0.032	0.023	24	
7468.31	N I	3	7468.08	0.052	0.036	16	
7499.85	He I	1/8	7499.83	0.050	0.035	17	
	?		7512.99	0.010	0.007	:	

Table 2 – *continued*

λ_0 (Å)	Ion	Multiplet	λ_{obs} (Å)	$F(\lambda)$	$I(\lambda)^a$	Error (per cent)^b	Notes
7706.74	O I	42	7706.76	0.022	0.015	33	
7751.10	[Ar III]	2F	7751.15	4.549	3.132	5	*c*
7771.94	O I	1	7771.85	0.052	0.036	16	*c*
7782.18	Mn I		7781.83	0.030	0.021	26	*g*
7790.60	Ar I		7790.54	0.034	0.023	23	
7801.79	V I		7801.50	0.016	0.011	:	*g*
7816.13	He I	1/7	7816.31	0.087	0.059	11	
7837.85	[Co I]		7837.44	0.053	0.036	16	
7862.75	Fe II]		7862.38	0.018	0.012	:	*g*
7959.70	N I		7959.49	0.057	0.039	15	*g*
8046.80	Si I	73	8046.11	0.031	0.021	25	*g*
8184.85	N I	2	8184.60	0.022	0.015	34	
8150.57	Si I	20	8150.24	0.016	0.011	:	
8210.72	N I	2	8210.26	0.014	0.009	:	
8216.28	N I	2	8216.05	0.059	0.039	15	
8223.14	N I	2	8222.88	0.066	0.044	13	
8257.85	H I	P37	8257.95	0.049	0.033	17	
8260.93	H I	P36	8260.93	0.058	0.039	15	
8264.28	H I	P35	8264.15	0.073	0.048	12	
8266.40	Ar I		8266.16	0.049	0.032	17	*g*
8267.94	H I	P34	8267.80	0.089	0.059	11	
8271.93	H I	P33	8271.85	0.119	0.079	9	
8276.31	H I	P32	8276.21	0.114	0.076	9	
8281.12	H I	P31	8280.91	0.193	0.128	7	
8286.43	H I	P30	8286.23	0.140	0.093	8	
8292.31	H I	P29	8292.19	0.162	0.108	7	
8298.83	H I	P28	8298.61	0.145	0.096	8	
8306.11	H I	P27	8306.05	0.095	0.063	11	*d*
8314.26	H I	P26	8314.09	0.218	0.144	7	
8323.42	H I	P25	8323.31	0.240	0.159	6	
8333.78	H I	P24	8333.64	0.256	0.169	6	
8334.75	Fe II]		8334.11	0.135	0.089	8	*g*
8345.55	H I	P23	–	–	–	–	*c*
8359.00	H I	P22	8358.88	0.329	0.217	6	
8361.67	HeI	1/6	8361.70	0.191	0.126	7	
8374.48	H I	P21	8374.34	0.353	0.232	6	
8387.77	Fe I		8387.31	0.044	0.029	18	*g*
8392.40	H I	P20	8392.26	0.460	0.302	6	
8397.	He I	6/19	8397.40	0.019	0.013	39	
8413.32	H I	P19	8413.19	0.504	0.330	5	
8437.96	H I	P18	8437.84	0.571	0.372	5	
8446.35	O I	4	8446.16	0.556	0.362	5	*c*
8446.36	O I	4					
8459.32	[Cr II]		8458.96	0.097	0.063	10	
8467.25	H I	P17	8467.15	0.627	0.408	5	
8486.	He I	6/16	8486.18	0.031	0.020	25	
8502.48	H I	P16	8502.36	0.840	0.543	5	*c*
8518.04	He I	2/8	8517.87	0.014	0.009	:	
8528.99	He I	6/15	8528.99	0.025	0.016	31	
8665.02	H I	P13	8664.93	2.131	1.348	5	*c*
8680.28	N I	1	8679.94	0.044	0.028	19	
8683.40	N I	1	8685.83	0.027	0.017	29	
8703.25	N I	1	8702.94	0.025	0.016	30	
8711.70	N I	1	8711.43	0.037	0.023	22	
8727.13	[C I]	3F	8726.68	0.239	0.150	7	
8733.43	He I	6/12	8733.37	0.052	0.033	16	
8750.47	H I	P12	8750.36	1.834	1.148	6	
8788.88	Cr II]		8788.81	0.071	0.044	13	*g*
8845.38	He I	6/11	8845.28	0.079	0.049	12	
8848.05	He I	7/11	8847.87	0.044	0.027	19	
8862.79	H I	P11	8862.66	2.492	1.538	6	

Table 2 – *continued*

λ_0 (Å)	Ion	Multiplet	λ_{obs} (Å)	$F(\lambda)$	$I(\lambda)^a$	Error (per cent)^b	Notes
8889.00	C II]		8888.48	0.042	0.026	20	*g*
8893.87	V I]		8893.46	0.104	0.064	10	*g*
8946.05	Fe II]		8945.87	0.053	0.032	16	*g*
8996.99	He I	6/10	8996.89	0.096	0.058	11	
9014.91	H I	P10	9014.80	3.083	1.873	6	
9019.19	Fe I		9018.95	0.112	0.068	10	*g*
9029.30	C II		9029.09	0.128	0.078	9	*g*
9063.29	He I	4/8	9063.16	0.058	0.035	15	
9068.90	[S III]	1F	9068.82	40.228	24.330	6	
9094.83	C I	3	9094.48	0.067	0.040	14	*c*
9111.81	C I	3	9111.42	0.041	0.025	20	
9113.70	Cl II]		9113.21	0.065	0.039	14	*g*
9123.60	[Cl II]	1F	9123.40	0.166	0.100	8	
9210.28	He I	6/9	9210.24	0.139	0.083	9	
9229.01	H I	P9	9228.89	4.463	2.672	6	
9507.82	Si I		9507.66	0.070	0.042	13	
9516.57	He I	1/5	9516.44	0.116	0.069	10	
9530.60	[S III]	1F	9530.87	94.238	55.914	6	
9545.97	H I	P8	9545.94	4.274	2.535	6	*d*
9702.62	He I	75	9702.92	0.039	0.023	:	*d*
9824.13	[C I]	1F	9823.76	0.809	0.480	6	
9876.87	Fe I]		9876.35	0.146	0.086	9	*g*
9850.24	[C I]	1F	9849.73	3.266	1.936	6	
9903.46	C II	17.02	9903.42	0.111	0.066	:	
9903.88	C II	17.02					
10 027.70	He I	6/7	10 027.54	0.292	0.173	7	
10 049.37	H I	P7	10 049.24	11.265	6.681	6	
10 320.49	[S II]	3F	10 320.28	1.011	0.600	6	
10 336.41	[S II]	3F	10 335.97	1.057	0.627	6	
			NGC 3603				
3686.83	H I	H19	3686.87	0.280	1.195	:	
3691.56	H I	H18	3691.73	0.309	1.311	37	
3697.15	H I	H17	3697.36	0.329	1.382	35	
3703.86	H I	H16	3704.04	0.360	1.485	32	
3705.04	He I	25	3705.22	0.140	0.576	:	
3711.97	H I	H15	3712.24	0.346	1.411	33	
3721.83	[S III]	2F	3722.00	0.774	3.119	17	
3721.94	H I	H14					
3726.03	[O II]	1F	3726.26	10.070	40.360	5	
3728.82	[O II]	1F	3728.95	6.256	24.990	5	
3734.37	H I	H13	3734.56	0.715	2.835	18	
3750.15	H I	H12	3750.43	1.017	3.951	14	
3770.63	H I	H11	3770.84	1.158	4.385	12	
3797.90	H I	H10	3798.09	1.517	5.553	10	
3819.61	He I	20	3819.83	0.379	1.352	31	
3835.39	H I	H9	3835.58	2.344	8.205	7	
3868.75	[Ne III]	1F	3868.95	10.895	36.682	4	
3888.65	He I	2	3889.18	4.627	15.221	4	
3889.05	H I	H8					
3964.73	He I	5	3964.97	0.298	0.899	11	
3967.46	[Ne III]	1F	3967.65	3.445	10.363	4	
3970.07	H I	H7	3970.28	5.560	16.672	4	
4009.22	He I	55	4009.45	0.098	0.281	25	
4023.98	He I	54	4023.55	0.023	0.065	:	
4026.08	N II	40	4026.43	0.889	2.489	6	
4026.21	He I	18					
4068.60	[S II]	1F	4068.84	0.342	0.906	10	
4076.35	[S II]	1F	4076.63	0.115	0.303	22	
4097.25	O II	20	4097.34	0.033	0.085	:	
4097.26	O II	48b					
4101.74	H I	H6	4101.95	10.261	26.083	3	

Table 2 – *continued*

λ_0 (Å)	Ion	Multiplet	λ_{obs} (Å)	$F(\lambda)$	$I(\lambda)^a$	Error (per cent)^b	Notes
4120.84	He I	16	4121.04	0.130	0.323	20	
4143.76	He I	53	4144.02	0.155	0.374	18	
4153.30	O II	19	4153.42	0.045	0.107	:	
4267.15	C II	6	4267.38	0.150	0.325	18	
4317.14	O II	2	4317.35	0.037	0.076	:	
4325.75	O II	2	4326.21	0.030	0.061	:	
4340.47	H I	H5	4340.70	25.687	51.824	3	
4345.55	O II	65c	4345.73	0.060	0.121	:	
4345.56	O II	2					
4349.43	O II	2	4349.50	0.074	0.148	:	
4363.21	[O III]	2F	4363.44	1.264	2.483	5	
4368.25	O I	5	4368.37	0.060	0.116	:	
4387.93	He I	51	4388.18	0.353	0.671	10	
4437.55	He I	50	4437.88	0.049	0.087	:	*e*
4471.48	He I	14	4471.75	3.129	5.274	3	
4562.60	Mg I]	1	4562.27	0.028	0.041	:	*g*
4571.10	Mg I]	1	4571.24	0.032	0.047	:	
4630.54	N II	5	4630.77	0.029	0.040	:	
4638.86	O II	1	4639.04	0.043	0.057	:	
4640.64	N III	2	4640.73	0.066	0.088	33	
4641.81	O II	1	4642.08	0.098	0.131	25	
4649.13	O II	1	4649.42	0.130	0.172	20	
4650.84	O II	1	4651.06	0.066	0.086	34	
4658.10	[Fe III]	3F	4658.42	0.216	0.264	14	
4661.63	O II	1	4661.84	0.085	0.111	28	
4676.24	O II	1	4676.42	0.032	0.040	:	
4696.36	O II	1	4696.61	0.030	0.037	:	*g*
4701.62	[Fe III]	3F	4701.90	0.071	0.083	30	
4711.37	[Ar IV]	1F	4711.46	0.204	0.249	14	
	[Ar IV]	Red component	4712.04	0.045	0.054	:	
4713.14	He I	12	4713.46	0.573	0.697	7	
4733.91	[Fe III]	3F	4734.15	0.040	0.048	:	
4740.16	[Ar IV]	1F	4740.32	0.173	0.203	16	
	[Ar IV]	Red component	4740.88	0.040	0.047	:	
4754.83	[Fe III]	3F	4755.06	0.050	0.055	:	
4861.33	H I	H4	4861.60	100.000	100.000	3	
4881.00	[Fe III]	2F	4881.35	0.115	0.113	22	
4921.93	He I	48	4922.21	1.382	1.278	4	
4924.50	[Fe III]	2F	4924.76	0.076	0.070	30	
4924.50	O II	28					
4931.32	[O III]	1F	4931.45	0.045	0.040	:	
4958.91	[O III]	1F	4959.20	204.749	180.464	3	
4985.90	[Fe III]	2F	4985.75	0.164	0.139	37	
4987.20	[Fe III]	2F	4987.85	0.280	0.238	25	
5006.84	[O III]	1F	5007.15	641.906	533.117	3	
5015.68	He I	4	5015.99	2.663	2.188	5	
5045.10	N II	4	5045.36	0.797	0.633	12	
5047.74	He I	47	5048.32	1.868	1.479	6	*e*
5055.98	Si II	5	5056.38	0.294	0.230	24	
5056.31	Si II	5					
5197.90	[N I]	1F	5198.06	0.439	0.294	18	
5200.26	[N I]	1F	5200.16	0.210	0.140	30	
5270.30	[Fe III]	1F	5270.81	0.218	0.151	30	
5517.71	[Cl III]	1F	5518.01	1.090	0.512	9	
5537.88	[Cl III]	1F	5538.19	1.425	0.655	8	
5666.64	N II	3	5666.91	0.109	0.043	:	
5754.64	[N II]	3F	5754.98	1.141	0.404	9	
5875.64	He I	11	5876.03	46.671	14.418	4	
5929.57	[Mn II]		5929.93	0.348	0.102	21	*g*
6300.30	[O I]	1F	6300.48	8.132	1.729	5	*c*
6312.10	[S III]	3F	6312.49	8.784	1.849	5	
6363.78	[O I]	1F	6363.95	2.720	0.549	6	

Table 2 – *continued*

λ_0 (Å)	Ion	Multiplet	λ_{obs} (Å)	$F(\lambda)$	$I(\lambda)^a$	Error (per cent)^b	Notes
6548.03	[N II]	1F	6548.52	35.669	6.227	5	
6562.82	H I	H3	6563.22	1639.4	283.100	5	
6578.05	C II	2	6578.43	1.464	0.250	9	
6583.41	[N II]	1F	6583.90	114.401	19.455	5	
6678.15	He I	46	6678.59	24.226	3.850	5	
6716.47	[S II]	2F	6716.87	9.100	1.409	5	
6730.85	[S II]	2F	6731.29	15.109	2.317	5	
6989.47	He I	1/12	6989.93	0.133	0.017	13	
7002.23	O I	21	7002.58	0.169	0.022	11	
7062.26	He I	1/11	7062.75	0.132	0.016	13	
7065.28	He I	10	7065.72	59.096	7.369	6	
7110.90	[Cr IV]	1F	7110.94	0.036	0.004	:	*g*
7135.78	[Ar III]	1F	7136.23	154.166	18.457	6	
7155.14	[Fe II]	14F	7155.69	0.179	0.021	11	
7160.58	He I	1/10	7161.04	0.278	0.033	9	
7231.34	C II	3	7231.75	0.761	0.086	7	
7236.19	C II	3	7237.01	1.582	0.179	6	
7254.15	O I	20	7254.90	0.301	0.034	9	
7254.45	O I	20					
7254.53	O I	20					
7281.35	He I	45	7281.82	6.843	0.754	6	
7298.05	He I	1/9	7298.53	0.357	0.039	8	
7318.39	[O II]	2F	7319.53	10.130	1.093	6	
7319.99	[O II]	2F	7320.61	30.523	3.293	6	
7329.66	[O II]	2F	7330.17	16.775	1.800	6	
7330.73	[O II]	2F	7331.25	16.608	1.781	6	
7377.83	[Ni II]	2F	7378.40	0.214	0.022	10	
7388.17	[Fe II]	14F	7388.67	0.028	0.003	35	
7411.61	[Ni II]	2F	7412.16	0.073	0.007	19	
7423.64	N I	3	7424.10	0.038	0.004	29	
7442.30	N I	3	7442.81	0.069	0.007	19	
7452.54	[Fe II]	14F	7453.02	0.067	0.007	20	
7468.31	N I	3	7468.78	0.078	0.008	19	
7499.85	He I	1/8	7500.34	0.584	0.057	7	
7504.94	O II		7505.36	0.074	0.007	19	
7530.54	[Cl IV]	1F	7530.77	0.674	0.065	8	
	[Cl IV]	Red component	7531.60	0.099	0.010	16	
7751.10	[Ar III]	2F	7751.60	53.803	4.658	6	
7816.13	He I	1/7	7816.65	1.023	0.086	7	
8045.63	[Cl IV]	1F	8045.92	1.042	0.080	7	
	[Cl IV]	Red component	8046.82	0.394	0.030	9	*f*
8057.	He I	4/18	8058.05	0.142	0.011	13	
8116.	He I	4/16	8116.98	0.169	0.013	12	
8155.66	He I	4/15	8156.10	0.173	0.013	12	
8188.01	N I	2	8188.55	0.196	0.014	11	
8203.85	He I	4/14	8204.41	0.176	0.013	12	
8210.72	N I	2	8211.31	0.065	0.005	20	
8216.28	N I	2	8216.92	0.163	0.012	12	
8223.14	N I	2	8223.66	0.182	0.013	12	
8245.64	H I	P42	8246.19	0.588	0.041	8	
8247.73	H I	P41	8248.29	0.651	0.045	8	
8249.20	H I	P40	8250.52	0.710	0.049	8	
8252.40	H I	P39	8253.00	0.752	0.052	8	
8255.02	H I	P38	8255.58	1.027	0.071	8	
8257.85	H I	P37	8258.39	1.270	0.088	7	
8260.93	H I	P36	8261.48	1.229	0.085	7	
8264.28	H I	P35	8264.89	1.362	0.094	7	*f*
8265.71	He I	4/13	8266.02	0.243	0.017	10	
8265.71	He I	2/9					
8267.94	H I	P34	8268.50	1.182	0.081	7	
8271.93	H I	P33	8272.54	1.073	0.073	7	

Table 2 – *continued*

λ_0 (Å)	Ion	Multiplet	λ_{obs} (Å)	$F(\lambda)$	$I(\lambda)^a$	Error (per cent)^b	Notes
8276.31	H I	P32	8276.94	1.239	0.085	7	
8281.12	H I	P31	8281.67	1.909	0.130	7	*c*
8286.43	H I	P30	8286.65	1.303	0.089	7	
8292.31	H I	P29	8292.88	1.794	0.122	7	
8298.83	H I	P28	8299.07	2.899	0.196	7	
8306.11	H I	P27	8306.69	2.160	0.145	7	
8314.26	H I	P26	8314.84	2.419	0.162	7	
8323.42	H I	P25	8323.99	2.670	0.177	7	
8333.78	H I	P24	8334.36	2.869	0.189	7	
8342.33	He I	4/12	8343.15	0.994	0.065	8	
8345.55	H I	P23	8346.14	3.204	0.210	7	
8359.00	H I	P22	8359.56	3.855	0.250	7	
8361.67	He I	1/6	8362.29	2.301	0.149	7	
8374.48	H I	P21	8375.03	4.043	0.259	7	
8376.	He I	6/20	8376.47	0.289	0.019	10	
8392.40	H I	P20	8392.97	4.802	0.303	7	
8397.	He I	6/19	8398.27	0.270	0.017	10	
8413.32	H I	P19	8413.88	5.683	0.352	7	
8422.	He I	6/18	8422.45	0.213	0.013	11	
8433.85	[Cl III]	3F	8434.33	0.277	0.017	10	
8437.96	H I	P18	8438.52	6.575	0.400	7	
8444.34	He I	4/11	8445.00	0.483	0.029	9	
8446.25	O I	4	8446.94	3.250	0.196	7	
8446.36	O I	4					
8467.25	H I	P17	8467.82	7.856	0.466	7	
8480.90	[Cl III]	3F	8481.39	0.252	0.015	11	
8486.	He I	6/16	8486.76	0.350	0.020	9	
8488.	He I	7/16	8489.36	0.145	0.008	14	
8500.00	[Cl III]	3F	8500.49	0.480	0.028	9	
8502.48	H I	P16	8503.05	9.437	0.543	7	
8518.04	He I	2/8	8518.68	0.247	0.014	11	
8528.99	He I	6/15	8529.56	0.460	0.026	9	
8531.48	He I	7/15	8532.22	0.271	0.015	10	
8665.02	H I	P13	8665.59	20.675	1.030	8	
8680.28	N I	1	8680.47	0.444	0.022	9	
8683.40	N I	1	8684.02	0.175	0.009	12	
8686.15	N I	1	8686.73	0.088	0.004	17	
8703.25	N I	1	8703.93	0.137	0.007	14	
8711.70	N I	1	8712.38	0.178	0.009	12	
8728.90	[Fe III]	8F	8729.93	0.166	0.008	13	
8728.90	N I	28					
8733.43	He I	6/12	8734.04	0.996	0.047	8	
8736.04	He I	7/12	8736.72	0.349	0.016	10	
8750.47	H I	P12	8751.07	26.668	1.234	8	
8776.77	He I	4/9	8777.33	0.821	0.037	9	
8816.82	He I	10/12	8817.18	0.163	0.007	13	
8829.40	[S III]	3F	8830.38	0.377	0.016	10	
8845.38	He I	6/11	8845.94	1.510	0.065	8	
8848.05	He I	7/11	8848.45	0.453	0.019	10	
8854.11	He I	5/11	8854.79	0.287	0.012	11	
8862.79	H I	P11	8863.39	36.948	1.563	8	
8914.77	He I	2/7	8915.34	0.512	0.021	9	
8930.97	He I	10/11	8931.36	0.185	0.007	12	
8996.99	He I	6/10	8997.58	2.088	0.081	8	
9014.91	H I	P10	9015.51	51.574	1.967	8	
9063.29	He I	4/8	9063.93	1.961	0.073	9	
9068.90	[S III]	1F	9069.68	793.638	29.363	8	*d*
9123.60	[Cl II]	1F	9124.23	0.272	0.010	11	
9210.28	He I	6/9	9210.96	2.954	0.103	9	
9213.20	He I	7/9	9213.84	0.883	0.031	9	
9226.62	[Fe II]		9227.05	0.143	0.005	14	

Table 2 – *continued*

λ_0 (Å)	Ion	Multiplet	λ_{obs} (Å)	$F(\lambda)$	$I(\lambda)^a$	Error (per cent)^b	Notes
9229.01	H I	P9	9229.64	79.747	2.759	9	
	?		9236.95	0.383	0.013	10	
9463.57	He I	1/5	9464.26	6.084	0.200	9	
9526.16	He I	6/8	9526.80	6.401	0.209	9	
9530.60	[S III]	1F	9531.62	2912.0	95.058	9	
9545.97	H I	P8	9546.68	110.044	3.588	9	
9603.44	He I	2/6	9603.92	0.683	0.022	10	
9702.62	He I	75	9702.88	0.747	0.024	9	
9824.13	[C I]	1F	9824.77	0.537	0.017	10	
9850.24	[C I]	1F	9850.92	2.283	0.074	9	
9903.46	C II	17.02	9903.96	3.416	0.111	9	*f*
9903.88	C II	17.02					
10 027.70	He I	6/7	10 028.42	11.220	0.365	9	
10 031.20	He I	7/7	10 031.86	3.573	0.116	9	
10 049.37	H I	P7	10 050.09	292.904	9.539	9	
10 138.42	He I	10/7	10 139.13	1.567	0.051	9	
10 311.53	He I	4/6	10 312.13	8.657	0.283	9	
10 320.49	[S II]	3F	10 321.15	15.068	0.492	9	
10 336.41	[S II]	3F	10 337.10	11.600	0.379	9	
10 370.50	[S II]	3F	10 371.16	6.658	0.217	9	

[a] c(Hβ), I(Hβ) values per nebula are: M16 (1.21, 7.331 $\times$ 10^{-12} erg cm^{-2} s^{-1}); M20 (0.36, 1.081 $\times$ 10^{-12} erg cm^{-2} s^{-1}); and NGC 3603 (2.36, 6.506 $\times$ 10^{-11} erg cm^{-2} s^{-1}).
[b] Colons indicate uncertainties larger than 40 per cent.
[c] Affected by telluric emission lines.
[d] Affected by atmospheric absorption bands.
[e] Affected by internal reflections or charge transfer in the CCD.
[f] Blend with an unknown line.
[g] Dubious identification.

derived following García-Rojas et al. (2004), adding quadratically the error due to flux calibration that has been estimated to be about 3 per cent, which corresponds to the standard deviation obtained from the calibration curves of the three standard stars.

A total of 256, 261 and 235 emission lines were measured in M16, M20 and NGC 3603, respectively. Most of the lines are permitted lines. We have measured 54 forbidden lines (CELs) in M16, 58 in M20 and 60 in NGC 3603. We have detected several semiforbidden lines: eight in M16, 12 in M20, and only two in NGC 3603 (see Table 2). Four lines detected in NGC 3603 were identified as red velocity components of highly ionized species (see Section 8 for a detailed discussion on these lines). In several cases, some identified lines were severely blended with telluric lines, making impossible their measurement. Other lines were strongly affected by atmospheric features in absorption or by internal reflections by charge transfer in the CCD, rendering their intensities unreliable. Also, several lines were labelled as dubious identifications and two emission lines could not be identified in any of the available references. All those lines are indicated in Table 2.

The identification and adopted laboratory wavelengths of the lines were obtained, following several previous identifications in the literature (see García-Rojas et al. 2004; Esteban et al. 2004, and references therein). Several identifications labelled as dubious in García-Rojas et al. (2004, 2005) have been updated in this work following a criterion based on the comparison of the radial velocity of the line with the lines of similar ionization potential.

We have assumed the standard dust extinction law for the Milky Way ($R_v = 3.1$) parametrized by Seaton (1979) for M20 and NGC 3603. A reddening coefficient of c(Hβ) = 0.36 $\pm$ 0.04 was determined for M20, by fitting the observed I(H Balmer lines)/I(Hβ) ratios (from H16 to Hβ) and I(H Paschen lines)/I(Hβ) (from P22 to P7), to the theoretical ones computed by Storey & Hummer (1995) for T_e = 10 000 K and n_e = 1000 cm^{-3} (see below). H I lines affected by blends or atmospheric absorption were not considered. Our derived c(Hβ) is slightly lower than previous determinations in M20, but it has been derived with a much larger number of H I lines: Hawley (1978) derived c(Hβ) = 0.42 and 0.48 for two slit positions with offsets of 33 arcsec south, 10 arcsec west, and 33 arcsec south, 25 arcsec east from our slit position; Lynds & O'Neil (1985) computed a value of c(Hβ) = 0.45 from long-slit spectroscopic data for a larger extension of the nebula.

Following the same method as for M20, we have derived c(Hβ) = 2.36 $\pm$ 0.06 for NGC 3603. Tapia et al. (2001) derived a c(Hβ) = 2.51 for a slit position 116 arcsec east and 12 arcsec north from our slit position. Melnick et al. (1989) derived an average c(Hβ) = 1.93 for four slit positions. Girardi et al. (1997) obtained c(Hβ) = 2.36 and 2.59 for two slit positions in NGC 3603 located near ours and using the extinction law of Savage & Mathis (1979). Even though the different extinction laws used are different, these values of c(Hβ) are in very good agreement with our value. Using the extinction law by Savage & Mathis (1979), we have obtained c(Hβ) = 2.29 $\pm$ 0.06 which is consistent with our adopted value.

On the other hand, Chini & Wargau (1990) confirmed an abnormal extinction of dense interstellar dust within M16 from photometric observations of the associated young stellar cluster NGC 6611. They found that deviations from the normal extinction law occur at wavelenghts shorter than 5500 Å, because of the higher size of the graphite grains. Following those authors, we have assumed the

Table 3. Plasma diagnostic.

Parameter	Line	Value		
		M16	M20	NGC 3603
n_e (cm^{-3})	[N I] (λ5198)/(λ5200)	1100^{+750}_{-400}	560^{+340}_{-220}	4000:
	[O II] (λ3726)/(λ3729)	1050 ± 250	240 ± 70	2300 ± 750
	[O II] (λ3726+λ3729)/(λ7320+λ7330)[a]			5300 ± 850
	[S II] (λ6716)/(λ6731)	1390 ± 550	320 ± 130	4150^{+3350}_{-1650}
	[Fe III]	$540^{+>1000}_{-500}$	560 ± 390	1330:[c]
	[Cl III] (λ5518)/(λ5538)	1370 ± 1000	350^{+780}_{-350}	5600^{+3900}_{-2400}
	[Ar IV] (λ4711)/(λ4740)	–	–	⩽ 4000
	n_e(adopted)	1120 ± 220	270 ± 60	5150 ± 750
T_e(K)	[N II] (λ6548+λ6583)/(λ5755)[a]	8450 ± 270	8500 ± 240	11050 ± 800
	[S II] (λ6716+λ6731)/(λ4069+λ4076)	7520 ± 430	6950 ±350	11050^{+3550}_{-2050}
	[O II] (λ3726+λ3729)/(λ7320+λ7330)[a]	8260 ± 400	8275 ± 400	12350 ± 1250
	T_e (low)	8350 ± 200	8400 ± 200	11400 ± 700
	[O III] (λ4959+λ5007)/(λ4363)	7650 ± 250	7800 ± 300	9060 ±200
	[Ar III] (λ7136+λ7751)/(λ5192)	–	8730 ±920[b]	–
	[S III] (λ9069+λ9532)/(λ6312)	8430 ± 450	8300 ± 400	8800 ± 500
	T_e(high)	7850 ± 220	7980 ± 250	9030 ± 200
	He I	7300 ± 350	7650 ± 300	8480 ± 200
	Balmer decrement	5450 ± 820	6000 ± 1300	–
	Paschen decrement	7200 ± 1300	5700 ± 1300	6900 ± 1100

[a]The recombination contribution to the auroral lines has been taken into account (see text).
[b]The [Ar III] λ7751 line is severely blended with a telluric line.
[c]Colons indicate very high uncertainties. This value has not been taken into account in the adopted average.

extinction law parametrized by Cardelli, Clayton & Mathis (1989) with the ratio of total to selective extinction, $R_v = 3.1$ for wavelengths higher than 5500 Å, and $R_v = 4.8$ for shorter wavelengths. From this extinction law and following the same procedure than for M20 and NGC 3603, we have derived c(Hβ) = 1.21 ± 0.06 for M16, assuming $T_e = 8000$ K and $n_e = 1000\,\mathrm{cm}^{-3}$ (Rodríguez 1998).

4 PHYSICAL CONDITIONS

4.1 Temperatures and densities

The large number of emission lines identified and measured in the spectra allows us to derive physical conditions using different emission-line ratios. The temperatures and densities are presented in Table 3. Most of the determinations were carried out with the IRAF task TEMDEN of the package NEBULAR (Shaw & Dufour 1995).

The methodology followed for the derivation of n_e and T_e, and the atomic data compilation used have been described in previous papers (i.e. García-Rojas et al. 2004, 2005). In the case of electron densities, ratios of CELs of several ions have been used. We have derived the [Fe III] density from the intensity of the brightest lines (which have errors equal or smaller than 30 per cent and that seem not to be affected by line blending,see Table 2) together with the computations of Rodríguez (2002). We have used four, six and four [Fe III] lines for M16, M20 and NGC 3603, respectively; the methodology consisted of adopting the density that minimized the dispersion of individual Fe^{++}/H^+ abundance ratios. All the computed values of n_e are consistent within the errors (see Table 3).

A weighted mean of n_e(O II), n_e(Fe III), n_e(Cl III) and n_e(S II) has been used to derive T_e(N II), T_e(O II), T_e(S II), T_e(O III), T_e(Ar III) and T_e(S III), and we iterated until convergence. For M20, which has a low ionization degree, this is the first time that it has been possible to derive temperatures associated with highly ionized species. The values adopted for n_e are shown in Table 3. We have excluded n_e(N I) from the average because this ion is representative of the very outer part of the nebula, and does not coexist with the other ions.

Electron temperatures have been derived from the ratio of CELs of several ions and making use of NEBULAR routines with upgraded atomic data for [S III] (see García-Rojas et al. 2005).

We have corrected T_e(O II) for the contribution to λλ7320+7330 due to recombination following the formula derived by Liu et al. (2001) (their equation 2). From our O II RLs, we have estimated contributions of about 3, 2 and 7 per cent for M16, M20 and NGC 3603, respectively.

Also, the contribution to the intensity of the [N II] λ5755 line due to recombination can be estimated from an expression given by Liu et al. (2001) (their equation 1). From our data, we have obtained a contribution of recombination of about 2 per cent, for M16 and NGC 3603, that does not affect significantly the temperature determination. For M20, the derived contribution was less than 0.1 per cent, which is absolutely negligible.[2]

Fig. 1 shows the spectral regions near the Balmer and the Paschen limits. The discontinuities can be clearly appreciated, except in the case of the Balmer limit in NGC 3603. Discontinuities are defined as $I_c(\mathrm{Bac}) = I_c(\lambda3646^-) - I_c(\lambda3646^+)$ and $I_c(\mathrm{Pac}) = I_c(\lambda8203^-) - I_c(\lambda8203^+)$, respectively. The high spectral resolution of the spectra permits to measure the continuum emission in zones very near to the discontinuity, minimizing the possible contamination of other

[2] Although the formation mechanism of N II permitted lines is mostly resonance fluorescence by the RL He I λ508.64 Å (Grandi 1976), we have estimated N^{++}/H^+ abundances from N II lines of multiplet 3, which is less affected by such effects. Anyway, the correction is in all the cases very small, and effects due to resonance fluorescence do not modify the derived temperature by more than 100 K.

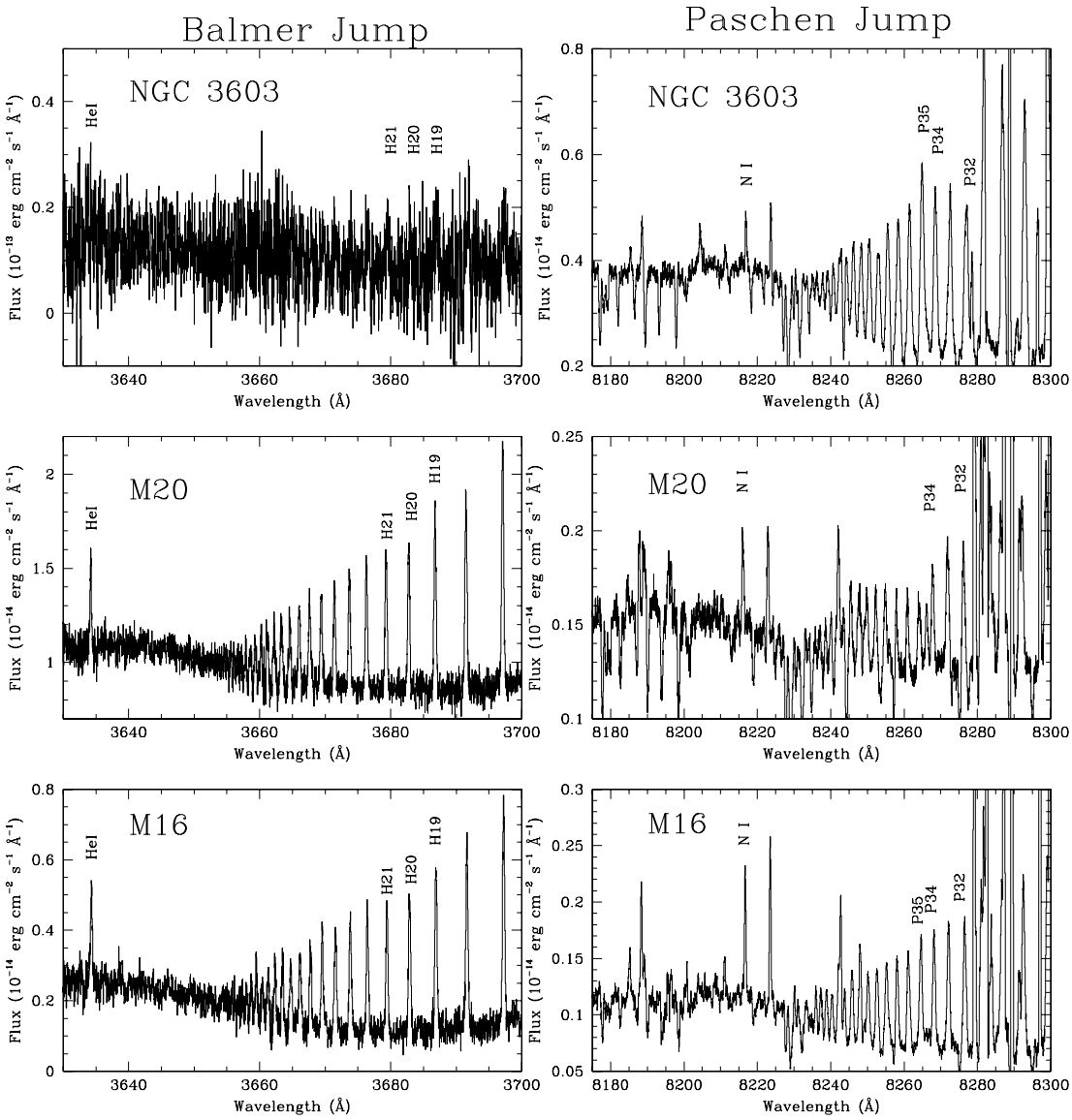

Figure 1. Section of the echelle spectra of the three nebulae including the Balmer (left-hand panel) and the Paschen (right-hand panel) limits (observed fluxes).

continuum contributions. In fact, on the blue part of Paschen discontinuity, we have selected a zone that is free of contamination by telluric absorption. That zone is between 8203 and 8209 Å. The uncertainty in the derived continua is the standard mean deviation of the averaged continua. On the red part, the measurement of the continuum is much easier, and could be computed as an average of the continua between the closest Paschen lines. We have obtained power-law fits to the relation between $I_c(\mathrm{Bac})/I(\mathrm{H}n)$ or $I_c(\mathrm{Pac})/I(\mathrm{P}n)$ and T_e for different n corresponding to different observed lines of both series. The emissivities as a function of electron temperature for the nebular continuum and the H I Balmer and Paschen lines have been taken from Brown & Mathews (1970) and Storey & Hummer (1995), respectively. The T_e(Bac) adopted is the average of the values using the lines from Hα to H10 (the brightest ones). In the case of T_e(Pac), the adopted value is the average of the individual temperatures obtained using the lines from P7 to P13 (the brightest lines of the series), excluding those lines whose intensity seems to be affected by telluric lines or sky absorption. To our knowledge, this is the first time that Balmer and Paschen temperatures have been derived for these three nebulae.

We have compared our averaged T_e(H I) with those derived from radio H I RLs. Caswell & Haynes (1987) obtained T_e(H I) = 6900 K for NGC 3603, the same value we derived for the Paschen temperature of this object; Reifenstein et al. (1970) derived T_e(H I) = 6100 ± 1500 K for M16 from the H109α radio RL, which is also in good agreement with our average temperature; however, for M20, Reifenstein et al. (1970) derived T_e(H I) = 7300 ± 2500, which is higher than the T_e(H I) we obtain, although it is compatible within the errors. Effects of scattered continuum light in the continua of Balmer and Paschen limits may be a reason of this discrepancy (see Section 9.1.1). However, aperture effects cannot be ruled out. Radio determinations usually refer to average values over large extensions of the nebula, instead our values refer to very small and particular zones of the nebulae. Another interesting comparison

is with T_e(H I) derived through radio continuum measurements. Shaver & Goss (1970) estimate T_e(H I) = 6800 ± 700 K for NGC 3603, from 408-MHz continuum measurements, which is in excellent agreement with the estimate through radio H I RLs and our own spectroscopic value.

Peimbert, Peimbert & Luridiana (2002) developed a method to derive the helium temperature, T_e(He I), in the presence of temperature fluctuations. Assuming a two-zone ionization scheme and the formulation of Peimbert et al. (2002), we have derived T_e(He I) = 7300 ± 350, 7650 ± 300 and 8480 ± 200 K for M16, M20 and NGC 3603, respectively. These results are higher than those derived from H I.

We have assumed a two-zone ionization scheme for the calculation of ionic abundances (see Section 5). We have adopted the average of electron temperatures obtained from [N II] and [O II] lines, as representative for the low-ionization zone designated T_e(low). The average of electron temperatures obtained from [O III] and [S III] lines has been assumed as representative of the high-ionization zone designated T_e(high) (see Table 3).

4.2 Temperature variations

Torres-Peimbert et al. (1980) proposed the presence of spatial temperature fluctuations (parametrized by t^2) as the cause of the discrepancy between abundance calculations based on CELs and RLs. This is due to the different dependence on the electron temperature of the CEL and RL emissivities. Assuming the validity of the temperature fluctuation paradigm, the comparison of the abundances determined from both kinds of lines for a given ion should provide an estimation of t^2. Also, Peimbert (1971) proposed that there is a dichotomy between T_e derived from the [O III] lines and from the hydrogen recombination continuum discontinuities, which is correlated with the discrepancy between CEL and RL abundances (e.g. Peimbert & Costero 1969; Torres-Peimbert et al. 1980; Liu et al. 2000; Tsamis et al. 2004), so the comparison between electron temperatures obtained from both the methods is an additional indicator of t^2. A complete formulation of temperature fluctuations has been developed by Peimbert (1967), Peimbert & Costero (1969) and Peimbert (1971) (see also Peimbert et al. 2002; Ruiz et al. 2003). Esteban (2002) discussed some of the different mechanisms proposed to explain the presence of temperature fluctuations in nebulae; it is beyond the scope of the present paper to treat this topic.

As we have assumed a two-zone ionization scheme, we have followed the re-formulation proposed by Peimbert, Peimbert & Ruiz (2000) and Peimbert et al. (2002) to derive the value of t^2, comparing the average of T_e(Bac) and T_e(Pac), with the combination of T_e([O II]) and T_e([O III]): T_e(O II+III), using equation (A1) of Peimbert et al. (2002).In Table 4, we include the different t^2 values that produce the agreement between the abundance determinations obtained from CELs and RLs of O^+ (for those objects where O I RLs have been measured) and O^{++}, as well as the values of t^2 obtained from the combination of T_e(O II+III) and the average values of T_e(Bac) and T_e(Pac). As it can be seen, the different t^2 values obtained are rather consistent. In Table 4, we also include the t^2 value obtained from the application of a maximum-likelihood method to search for the physical conditions, including He^+/H^+ ratios and optical depths, that would be a simultaneous fit to all the measured lines of He I (see Section 5.1). Finally, in Table 4 we show the final adopted values, which are error-weighted averages.

Table 4. t^2 parameter.

Method	t^2		
	M16	M20	NGC 3603
O^{++} (R/C)	0.046 ± 0.007	0.038 ± 0.016	0.042 ± 0.009
O^+ (R/C)	–	0.032 ± 0.020	–
He^+	0.017 ± 0.013	0.017 ± 0.010	0.032 ± 0.014
Bac/Pac–FL	0.045 ± 0.014	0.049 ± 0.019	0.056 ± 0.023
Adopted	0.039 ± 0.006	0.029 ± 0.007	0.040 ± 0.008

5 IONIC ABUNDANCES

5.1 He^+ abundance

We have measured 47, 53 and 64 He I emission lines in the spectra of M16, M20 and NGC 3603, respectively. These lines arise mainly from recombination, but they can be affected by collisional excitation and self-absorption effects. We have determined the He^+/H^+ ratio from a maximum-likelihood method (e.g. Peimbert et al. 2000), using the n_e given in Table 3, and T(O II+III) = 8130 K for M16, T(O II+III) = 8200 K for M20, and T(O II+III) = 9600 K for NGC 3603 (see Section 4.2). We have used the effective recombination coefficients of Storey & Hummer (1995) for H I and those of Smits (1996) and Benjamin, Skillman & Smits (1999) for He I. The collisional contribution was estimated from Sawey & Berrington (1993) and Kingdon & Ferland (1995), and the optical depth in the triplet lines was derived from the computations by Benjamin, Skillman & Smits (2002).

In Table 5, we have included the He^+/H^+ ratios we have obtained for the individual He I lines not affected by line blending and with the highest S/N. We have excluded He I λ5015, because it could suffer self-absorption effects from the 2^1S metastable level, as was already pointed out by Esteban et al. (2004). We have also excluded λ3889 for M16 and NGC 3603, because it is severely blended with the Balmer H8 line. We have performed a χ^2 optimization of the values given in the table, and we have obtained a χ^2 parameter of 8.3, 15.1 and 9.63 for M16, M20 and NGC 3603, respectively; these

Table 5. He^+ abundance.

Line	He^+/H^+[a]		
	M16	M20	NGC 3603
3819.61	827 ± 50	731 ± 44	1014 ± 314
3888.65	–	695 ± 21	–
3964.73	797 ± 32	749 ± 30	820 ± 90
4026.21	834 ± 25	756 ± 22	1043 ± 63
4387.93	777 ± 31	678 ± 41	1067 ± 107
4471.09	758 ± 23	690 ± 21	998 ± 30
4713.14	794 ± 32	674 ± 40	1001 ± 70
4921.93	757 ± 23	723 ± 22	926 ± 37
5875.64	761 ± 23	672 ± 19	921 ± 37
6678.15	751 ± 30	702 ± 28	911 ± 46
7065.28	781 ± 39	703 ± 28	956 ± 57
7281.35	831 ± 41	787 ± 39	957 ± 57
Adopted[b]	781 ± 12	711 ± 10	961 ± 17

[a]In units of 10^{-4}, for τ_{3889} = 2.99 ± 0.85, 2.09 ± 0.49 and 12.12 ± 1.00, and t^2 = 0.039 ± 0.006, 0.029 ± 0.007 and 0.040 ± 0.008. Uncertainties correspond to line-intensity errors.
[b]It includes all the relevant uncertainties in emission-line intensities, n_e, τ_{3889} and t^2.

Table 6. Ionic abundances from CELs[a].

Ion	M16		M20		NGC 3603	
	$t^2 = 0.000$	$t^2 = 0.039 \pm 0.006$	$t^2 = 0.000$	$t^2 = 0.029 \pm 0.007$	$t^2 = 0.000$	$t^2 = 0.040 \pm 0.008$
N^0	6.15 ± 0.06	6.33 ± 0.07	5.90 ± 0.07	6.03 ± 0.08	5.65 ± 0.11	5.75 ± 0.11
N^+	7.71 ± 0.05	7.88 ± 0.06	7.55 ± 0.04	7.67 ± 0.05	6.45 ± 0.07	6.55 ± 0.07
O^0	7.23 ± 0.05	7.40 ± 0.06	6.60 ± 0.05	6.72 ± 0.06	6.32 ± 0.09	6.42 ± 0.09
O^+	8.47 ± 0.08	8.66 ± 0.09	8.46 ± 0.07	8.59 ± 0.08	7.44 ± 0.11	7.54 ± 0.11
O^{++}	7.85 ± 0.07	8.18 ± 0.10	7.67 ± 0.08	7.90 ± 0.10	8.42 ± 0.05	8.68 ± 0.08
Ne^{++}	7.01 ± 0.07	7.38 ± 0.10	6.55 ± 0.09	6.80 ± 0.11	7.72 ± 0.05	8.00 ± 0.08
S^+	6.32 ± 0.05	6.49 ± 0.06	6.17 ± 0.05	6.29 ± 0.06	5.09 ± 0.10	5.18 ± 0.10
S^{++}	6.84 ± 0.06	7.22 ± 0.10	6.79 ± 0.06	7.09 ± 0.10	6.83 ± 0.04	7.11 ± 0.09
Cl^+	4.77 ± 0.05	4.91 ± 0.07	4.75 ± 0.05	4.85 ± 0.07	3.46 ± 0.07	3.54 ± 0.07
Cl^{++}	5.04 ± 0.06	5.36 ± 0.08	4.99 ± 0.07	5.21 ± 0.08	5.06 ± 0.05	5.30 ± 0.08
Cl^{3+}	–	–	–	–	3.86 ± 0.04	4.06 ± 0.07
Ar^{++}	6.25 ± 0.05	6.53 ± 0.08	6.17 ± 0.06	6.36 ± 0.08	6.35 ± 0.04	6.56 ± 0.07
Ar^{3+}	3.89 ± 0.22	4.23 ± 0.23	4.01 ± 0.18	4.24 ± 0.19	4.78 ± 0.06	5.04 ± 0.08
Fe^+	4.62:	4.78:	4.51:	4.62:	4.04:	4.13:
Fe^{++}	5.07 ± 0.04	5.41 ± 0.08	5.23 ± 0.10	5.47 ± 0.12	5.24 ± 0.06	5.50 ± 0.09

[a]In units of $12 + \log(X^m/H^+)$.

values indicate a reasonable goodness of the fits for a system with 9 degrees of freedom.

5.2 Ionic abundances from CELs

Ionic abundances of N^+, O^+, O^{++}, Ne^{++}, S^+, S^{++}, Cl^+, Cl^{++}, Cl^{3+} Ar^{++} and Ar^{3+} have been determined from CELs, using the IRAF package NEBULAR, except for Cl^+ (see García-Rojas et al. 2004). Additionally, we have determined the ionic abundances of Fe^{++}, which we will discuss further on. Ionic abundances are listed in Table 6 and correspond to the mean value of the abundances derived from all the individual lines of each ion observed (weighted by their relative strengths).

To derive the abundances for $t^2 > 0.00$ (see Section 4), we used the abundances for $t^2 = 0.00$ and the formulation of by Peimbert (1967) and Peimbert & Costero (1969). For other t^2 values, it is possible to interpolate or extrapolate the values presented in Table 6.

Many [Fe II] lines have been identified in our spectra, but are severely affected by fluorescence effects (Rodríguez 1999a; Verner et al. 2000). The [Fe II] λ8617 Å line is almost insensitive to fluorescence effects, but unfortunately it is in one of our narrow observational gaps. We have also measured [Fe II] λ7155, a line which does not seem to be affected by fluorescence effects (Rodríguez 1996). We have derived the Fe^+ abundance from this line, assuming that $I(\lambda7155)/I(\lambda8616) \sim 1$ (Rodríguez 1996), and using the calculations of Bautista & Pradhan (1996). We find $Fe^+/H^+ \sim 4.2 \times 10^{-8}$, 3.2×10^{-8} and 1.1×10^{-8} for M16, M20 and NGC 3603, respectively. In NGC 3603, the Fe^+ abundance is much lower than that of Fe^{++} (see Table 6). Therefore, in what follows the Fe^+ abundance will be considered negligible for this object.

The calculations for Fe^{++} have been done with a 34-level model-atom that uses the collision strengths of Zhang (1996) and the transition probabilities of Quinet (1996). We have used five [Fe III] lines for M16, six for M20 and five for NGC 3603, that do not seem to be affected by line blending. The Fe^{++} abundances are also included in Table 6.

5.3 Ionic abundances from recombination lines

We have measured a large number of permitted lines of heavy-element ions such as O I, O II, C I, C II, S II, N I, N II, Ar I, Si I, Si II and Fe I; many of them detected for the first time in these nebulae. Unfortunately, most permitted lines are affected by fluorescence effects or blended with telluric emission lines making their intensities unreliable. Detailed discussions on the mechanism of formation of the permitted lines can be found in Esteban et al. (1998, 2004, and references therein).

For the first time for these nebulae, we have been able to measure the ionic abundance ratios of O^+/H^+, O^{++}/H^+ and C^{++}/H^+ from pure RLs. We have computed the abundances using T_e(low) (for O^+/H^+), T_e(high) (for O^{++}/H^+ and C^{++}/H^+) and n_e from Table 3. Atomic data and methodology are the same than in García-Rojas et al. (2004). Although part of these ionic abundances were presented in a previous work of our group (Esteban et al. 2005), we give here the details of their derivation.

Eight permitted lines of C II have been measured in M16 and M20, and only five in NGC 3603. Lines of multiplets 6, 17.02 and 17.04 are 3d–4f transitions and are, in principle, excited by pure recombination (see Grandi 1976). Unfortunately, only multiplet 6 is usable because the lines of the other multiplets are affected by blending with atmospheric spectral features or CCD charge-transfer effects, so we have adopted the C^{++}/H^+ ratio given by that multiplet (see Table 7).

The O^+ abundance was derived from the O I λ7771.94 Å line, and was only reliable for M20, because the spectral zone of multiplet 1 is strongly affected by telluric lines. The abundance derived from this line is case-independent, and recombination is its formation mechanism because the line corresponds to a quintuplet transition, while the ground term of this ion is a triplet. The O^+/H^+ ratios are presented in Table 8.

We have measured several lines of multiplet 1 of O II. As it has been pointed out by Tsamis et al. (2003) and Ruiz et al. (2003), the upper levels of the transitions of multiplet 1 of O II are not in local thermodynamic equilibrium (LTE) for densities $n_e < 10\,000$ cm^{-3}, and the abundances derived from each individual line could differ by factors as large as 4. We have applied the non-local thermodynamic equilibrium (NLTE) corrections estimated by Peimbert, Peimbert & Ruiz (2005) to our data, and the abundances obtained from the individual lines are in good agreement and also agree with the abundance derived using the sum of all the lines of the multiplet, which is not affected by NLTE effects. On the other hand, Tsamis et al. (2003) pointed out that, in the presence of absorption-line features in the

Table 7. C^{++}/H^+ abundance ratio from C II lines.

		M16			M20			NGC 3603		
		$I(\lambda)/I(H\beta)$	C^{++}/H^+ ($\times10^{-5}$)		$I(\lambda)/I(H\beta)$	C^{++}/H^+ ($\times10^{-5}$)		$I(\lambda)/I(H\beta)$	C^{++}/H^+ ($\times10^{-5}$)	
Multiplet	λ_0	($\times10^{-2}$)	A	B	($\times10^{-2}$)	A	B	($\times10^{-2}$)	A	B
2	6578.05	0.310 ± 0.019	365 ± 22	60 ± 4	0.356 ± 0.021	414 ± 25	68 ± 4	0.250 ± 0.023	264 ± 24	47 ± 4
3	7231.12	0.096 ± 0.007	2533 ± 177	36 ± 3	0.075 ± 0.007	1971 ± 177	28 ± 3	0.086 ± 0.006	2300 ± 161	33 ± 2
	7236.19	0.178 ± 0.012	2660 ± 200	38 ± 2	0.126 ± 0.009	1884 ± 132	27 ± 2	0.179 ± 0.011	2705 ± 162	38 ± 2
	Sum		2614 ± 132	37 ± 1		1915 ± 106	27 ± 1		2558 ± 115	36 ± 1
4	3918.98	0.138 ± 0.018	2840 ± 369	900 ± 117	0.094 ± 0.019	1885 ± 377	595 ± 119	–	–	–
	3920.68	0.162 ± 0.019	1660 ± 199	525 ± 63	0.141 ± 0.020	1420 ± 199	450 ± 63	–	–	–
	Sum		2060 ± 175	650 ± 55		1575 ± 176	500 ± 56	–	–	–
6	4267.26	0.272 ± 0.019	25 ± 2	**25 ± 2**	0.170 ± 0.020	15 ± 2	**15 ± 2**	0.325 ± 0.059	31 ± 6	**30 ± 5**
17.02	9903.46	0.037 ± 0.005[a]	13 ± 2	–	0.066:	24:	–	0.111 ± 0.010[b]	43 ± 4	–
17.04	6461.95	0.032 ± 0.012	28 ± 10	–	0.043 ± 0.011[c]	38 ± 10	–	–	–	–
	Adopted		25 ± 2			15 ± 2			30 ± 5	

[a] Affected by atmospheric absorption bands.
[b] Blend with an unidentified line.
[c] Affected by internal reflections or charge transfer in the CCD.

Table 8. O^+/H^+ ratio from O I permitted lines.[a]

		M16			M20			NGC 3603		
		$I(\lambda)/I(H\beta)$	O^+/H^+ ($\times10^{-5}$)		$I(\lambda)/I(H\beta)$	O^+/H^+ ($\times10^{-5}$)		$I(\lambda)/I(H\beta)$	O^+/H^+ ($\times10^{-5}$)	
Multiplet	λ_0	($\times10^{-2}$)	A	B	($\times10^{-2}$)	A	B	($\times10^{-2}$)	A	B
1	7771.94	0.026 ± 0.006[b]	$26 \pm 6/34 \pm 8$	–	0.036 ± 0.006	$36 \pm 6/47 \pm 8$	–	–	–	–
4	8446.48	0.482 ± 0.034	$1849 \pm 129/$ 2717 ± 190	$413 \pm 29/$ 546 ± 38	0.362 ± 0.018	$1383 \pm 69/$ 2052 ± 103	$311 \pm 16/$ 412 ± 21	0.196 ± 0.014	$728 \pm 51/$ 1165 ± 82	$171 \pm 12/$ 2325 ± 163
	Adopted		30 ± 7			42 ± 7			–	

[a] Recombination coefficients by Pequignot, Petitjean & Boisson (1991)/Escalante & Victor (1992).
[b] Blended with telluric emission lines.

multiplet 1 spectral range, the emission lines could be attenuated. This effect can be very important in extragalactic objects, and it can only be corrected if the stars are resolved, or if synthetic spectra are available. In our case, our high-resolution spectra show, when compared with the spectrum of HD164492 (kindly provided by S. Simón-Díaz), the main ionizing source of M20, that the continuum does not affect the measurement of multiplet 1 O II emission-line fluxes, in spite of the large contribution of dust-scattered light to the nebular continuum (see Fig. 2 and Section 9.1.1). Indeed, the situation may be quite different in the case of low spectral resolution observations, as was the case of Tsamis et al. (2003) for 30 Dor and LMC N11B. The O^{++}/H^+ ratios for the three nebulae are presented in Table 9.

6 TOTAL ABUNDANCES

We have adopted a set of ionization correction factors (ICFs) to correct for the unseen ionization stages and then derive the total gaseous abundances of the chemical elements we have studied. We have adopted essentially the ICF scheme used by García-Rojas et al. (2005) for all the elements, but we will discuss some special cases.

The absence of He II lines in our spectra indicates that He^{++}/H^+ is negligible. However, the total helium abundance has to be corrected for the presence of neutral helium. Based on the ICF(He^0) given by Peimbert, Torres-Peimbert & Ruiz (1992) and with our data, the ICF(He^0) amounts to 1.18 ± 0.05, 1.16 ± 0.05 and 1.007 ± 0.002 for $t^2 > 0.00$, for M16, M20 and NGC 3603, respectively.

For all the nebulae, we have derived the O/H ratio from CELs, from the combination of O^{++}/H^+ ratio from RLs and O^+/H^+ ratio from CELs and the assumed t^2 (for M16 and NGC 3603) and, for the first time for M20, from pure RLs of O^+ and O^{++}. In Table 10, we show the total abundances obtained in our nebulae for $t^2 = 0.00$ and $t^2 > 0.00$.

For neon, we have used the ICF proposed by Peimbert & Costero (1969):

$$\frac{N(\mathrm{Ne})}{N(\mathrm{H})} = \left[\frac{N(\mathrm{O}^+) + N(\mathrm{O}^{++})}{N(\mathrm{O}^{++})}\right] \frac{N(\mathrm{Ne}^{++})}{N(\mathrm{H}^+)}. \quad (1)$$

Nevertheless, this ICF underestimates the Ne/H abundance for nebulae of low degree of ionization, because a considerable fraction of Ne^+ coexists with O^{++} (see Torres-Peimbert & Peimbert 1977; Peimbert et al. 1992). This is the case for M16 and M20. Based on the O^+/O ratio, the data and the prescriptions by Torres-Peimbert & Peimbert (1977), we estimate that the values of ICF(Ne) should be about 0.14 ± 0.1 dex for M16, and 0.42 ± 0.1 dex for M20 higher than those provided by equation (1) for $t^2 = 0.00$. From these values of ICF(Ne), we derive an Ne/O ratio of about 0.2 for both regions. This ratio is in excellent agreement with the Ne/O ratios derived for M17 by Peimbert et al. (1992), and by us for NGC 3603, where most of the O and Ne are twice ionized and the ICF(Ne) is very small. Given the high ionization degree for NGC 3603, equation 1 is a good approximation to the fraction of Ne^+ in this nebula.

We have measured lines of two ionization stages of chlorine in M16 and M20: Cl^+ and Cl^{++}. The Cl abundance has been assumed to be equal to the sum of these ionic abundances without taking into account the Cl^{3+} fraction. This assumption seems reasonable taking into account the small Cl^{3+}/Cl^{++} ratio found for M17 ($\sim$0.03, see

Table 9. O^{++}/H^+ ratio from O II permitted lines[a].

Multiplet	λ_0	$I(\lambda)/I(H\beta)$ ($\times10^{-2}$)	M16 O^{++}/H^+ ($\times10^{-5}$) A	M16 O^{++}/H^+ ($\times10^{-5}$) B	$I(\lambda)/I(H\beta)$ ($\times10^{-2}$)	M20 O^{++}/H^+ ($\times10^{-5}$) A	M20 O^{++}/H^+ ($\times10^{-5}$) B	$I(\lambda)/I(H\beta)$ ($\times10^{-2}$)	NGC 3603 O^{++}/H^+ ($\times10^{-5}$) A	NGC 3603 O^{++}/H^+ ($\times10^{-5}$) B
1[b]	4638.85	0.040 ± 0.010	37 ± 9/24 ± 6	35 ± 9/23 ± 6	–	–	–	0.057:	52:/43:	50:/41:
	4641.81	0.034 ± 0.010	13 ± 3/15 ± 4	13 ± 3/14 ± 4	0.030 ± 0.015	12 ± 6/14 ± 7	11 ± 6/13 ± 7	0.131 ± 0.033	49 ± 12/51 ± 13	47 ± 12/49 ± 12
	4649.14	0.056 ± 0.011	12 ± 2/20 ± 4	11 ± 2/19 ± 4	0.036 ± 0.018	8 ± 4/20 ± 10	7 ± 4/19 ± 10	0.172 ± 0.034	36 ± 7/42 ± 8	35 ± 7/41 ± 8
	4650.84	0.050 ± 0.011	49 ± 11/28 ± 6	47 ± 11/27 ± 6	0.030 ± 0.015	17 ± 9/8 ± 4	16 ± 8/7 ± 4	0.086 ± 0.029	84 ± 28/65 ± 22	81 ± 27/63 ± 21
	4661.64	0.038 ± 0.010	31 ± 8/20 ± 5	30 ± 8/19 ± 5	0.018 ± 0.014	15 ± 12/8 ± 6	14 ± 11/8 ± 6	0.111 ± 0.031	90 ± 25/74 ± 21	87 ± 24/72 ± 20
	4676.24	–	–	–	–	–	–	0.040:	42:/44:	41:/43:
	4696.36	–	–	–	–	–	–	0.037[c]:	381:/325:	368:/304:
	Sum		21 ± 2	**20 ± 2**		11 ± 5	**10 ± 5**		53 ± 6	**51 ± 6**
2	4349.43							0.148:	32:	31:
	Adopted			**20 ± 2**			**10 ± 5**			**51 ± 6**

[a]Except in the case of M20, only lines with intensity uncertainties lower than 40 per cent have been considered (see text).
[b]Not corrected from NLTE effects/corrected from NLTE effects (see text).
[c]Probably is a misidentification.

Esteban et al. 1999a), for the Orion nebula (∼0.04, see Esteban et al. 2004), for NGC 3576 (∼0.02, see García-Rojas et al. 2004), and for NGC 3603 (∼0.06, this work) and the lower ionization degree of M16 and M20 with respect to those nebulae. In NGC 3603, we have detected three ionization stages of chlorine, and the total abundance includes the sum of the Cl^+, Cl^{++} and Cl^{3+} abundances. Using the ICF by Peimbert & Torres-Peimbert (1977) to correct for the the presence of Cl^{3+}, we have obtained abundances 0.13 and 0.07 dex higher for M16 and M20, and 0.02 dex lower for NGC 3603, showing that this ICF scheme is a good approximation when [Cl IV] lines are not detected in the spectrum of H II regions with high degree of ionization; however, it overestimates the contribution of Cl^{3+} for the low-ionization regime.

We have measured lines of two stages of ionization of iron: Fe^+ and Fe^{++}. As we have commented in Section 5.2, the Fe^+ abundance is somewhat uncertain, so we have used the ICF scheme by Rodríguez & Rubin (2005) (based on photoionization models) to derive the total Fe/H ratio from the Fe^{++} abundance, which is given by:

$$\frac{N(\mathrm{Fe})}{N(\mathrm{H})} = 0.9 \left[\frac{N(\mathrm{O}^+)}{N(\mathrm{O}^{++})}\right]^{0.08} \left[\frac{N(\mathrm{Fe}^{++})}{N(\mathrm{O}^+)}\right] \left[\frac{N(\mathrm{O})}{N(\mathrm{H})}\right]. \quad (2)$$

In the case of high-ionization-degree nebulae, Rodríguez & Rubin (2005) used a further relation based on an observational fit, which is given by:

$$\frac{N(\mathrm{Fe})}{N(\mathrm{H})} = 1.1 \left[\frac{N(\mathrm{O}^+)}{N(\mathrm{O}^{++})}\right]^{0.58} \left[\frac{N(\mathrm{Fe}^{++})}{N(\mathrm{O}^+)}\right] \left[\frac{N(\mathrm{O})}{N(\mathrm{H})}\right]. \quad (3)$$

This last relation has been applied to obtain the Fe/H ratio of NGC 3603. The discrepancy observed between the Fe abundance obtained by making use of equation (2) or (3) for high-ionization-degree nebulae (e.g. see NGC 3603 Fe abundance on Table 10) has been extensively discussed by Rodríguez & Rubin (2005). From Table 10, it is clear that the sum of Fe^+ and Fe^{++} abundances for M16 and M20, respectively, are almost coincident with those derived using an ICF. In fact, for these regions, it is not expected a large contribution of Fe^{3+} to the total abundance, due to their low ionization degree. This is not true for objects with high ionization degree as NGC 3603, for which the fraction of Fe^{+3} is expected to be large; this is reflected in the large difference between the two values of Fe/H ratio given in Table 10. It is obvious that the sum of Fe^+ and Fe^{++} abundances is not applicable for this object; we must rely on the results obtained assuming an ICF.

7 DEUTERIUM BALMER LINES IN M16 AND M20

Hébrard et al. (2000) reported the detection of deuterium Balmer lines in the spectrum of M16 and M20. These authors detected from Dα to Dγ in M16 and only Dα in M20. We have detected several deuterium Balmer lines in M16 – from Dα to Dδ, and in M20 – from Dα to Dγ; these lines appear as very weak emission features in the blue wings of the corresponding H I Balmer lines (see Figs 3 and 4). The apparent shifts in radial velocity of these lines with respect to the hydrogen ones are $-76.5\,\mathrm{km\,s^{-1}}$ for M16 and $-90.8\,\mathrm{km\,s^{-1}}$ for M20, which are roughly consistent with the expected isotopic shift of deuterium, $-81.6\,\mathrm{km\,s^{-1}}$.

We have excluded the possibility that these weak features are high-velocity components of hydrogen following the same criteria as García-Rojas et al. (2005) for the case of S311. The first criterion

Table 10. Total gaseous abundances.

Element	M16		M20		NGC 3603	
	$t^2 = 0.000$	$t^2 = 0.039 \pm 0.006$	$t^2 = 0.000$	$t^2 = 0.029 \pm 0.007$	$t^2 = 0.000$	$t^2 = 0.040 \pm 0.008$
He	11.01 ± 0.02	10.97 ± 0.02	10.95 ± 0.06	10.92 ± 0.06	10.99 ± 0.01	10.99 ± 0.01
C	8.76 ± 0.06	8.76 ± 0.06	8.69 ± 0.08	8.69 ± 0.08	8.51 ± 0.07	8.51 ± 0.07
N	7.84 ± 0.06	8.07 ± 0.12	7.67 ± 0.05	7.83 ± 0.07	7.62 ± 0.13	7.89 ± 0.14
O	8.56 ± 0.07	8.78 ± 0.07	8.53 ± 0.06	8.67 ± 0.07	8.46 ± 0.05	8.71 ± 0.07
O[a]	8.81 ± 0.07	8.81 ± 0.07	8.71 ± 0.07	8.71 ± 0.07	8.72 ± 0.05	8.72 ± 0.05
Ne	7.86 ± 0.15	8.08 ± 0.17	7.83 ± 0.16	7.97 ± 0.18	7.76 ± 0.08	8.03 ± 0.11
S	6.96 ± 0.05	7.29 ± 0.08	6.88 ± 0.05	7.12 ± 0.09	7.03 ± 0.05	7.36 ± 0.08
Cl[b]	5.23 ± 0.04	5.49 ± 0.07	5.19 ± 0.05	5.37 ± 0.06	5.09 ± 0.05	5.33 ± 0.07
Ar	6.70 ± 0.07	6.84 ± 0.08	6.65 ± 0.06	6.70 ± 0.11	6.37 ± 0.15	6.58 ± 0.17
Fe[c]	5.17 ± 0.11	5.53 ± 0.13	5.31 ± 0.13	5.56 ± 0.15	$6.14 \pm 0.16/5.74 \pm 0.10$	$6.53 \pm 0.19/6.05 \pm 0.10$
Fe[d]	5.20 ± 0.06	5.51 ± 0.07	5.31 ± 0.09	5.52 ± 0.10	5.27 ± 0.06	5.52 ± 0.09

[a]For M20, O^+/H^+ and O^{++}/H^+ from RLs. For M16 and NGC 3603, O^{++}/H^+ from RLs and O^+/H^+ from CELs and t^2.
[b]For NGC 3603, from $Cl^+/H^+ + Cl^{++}/H^+ + Cl^{3+}/H^+$. For M16 and M20, from $Cl^+/H^+ + Cl^{++}/H^+$.
[c]ICF from equation (2) for M16 and M20; ICF from equation (2)/equation (3) for NGC 3603.
[d]$Fe/H = Fe^+/H^+ + Fe^{++}/H^+$.

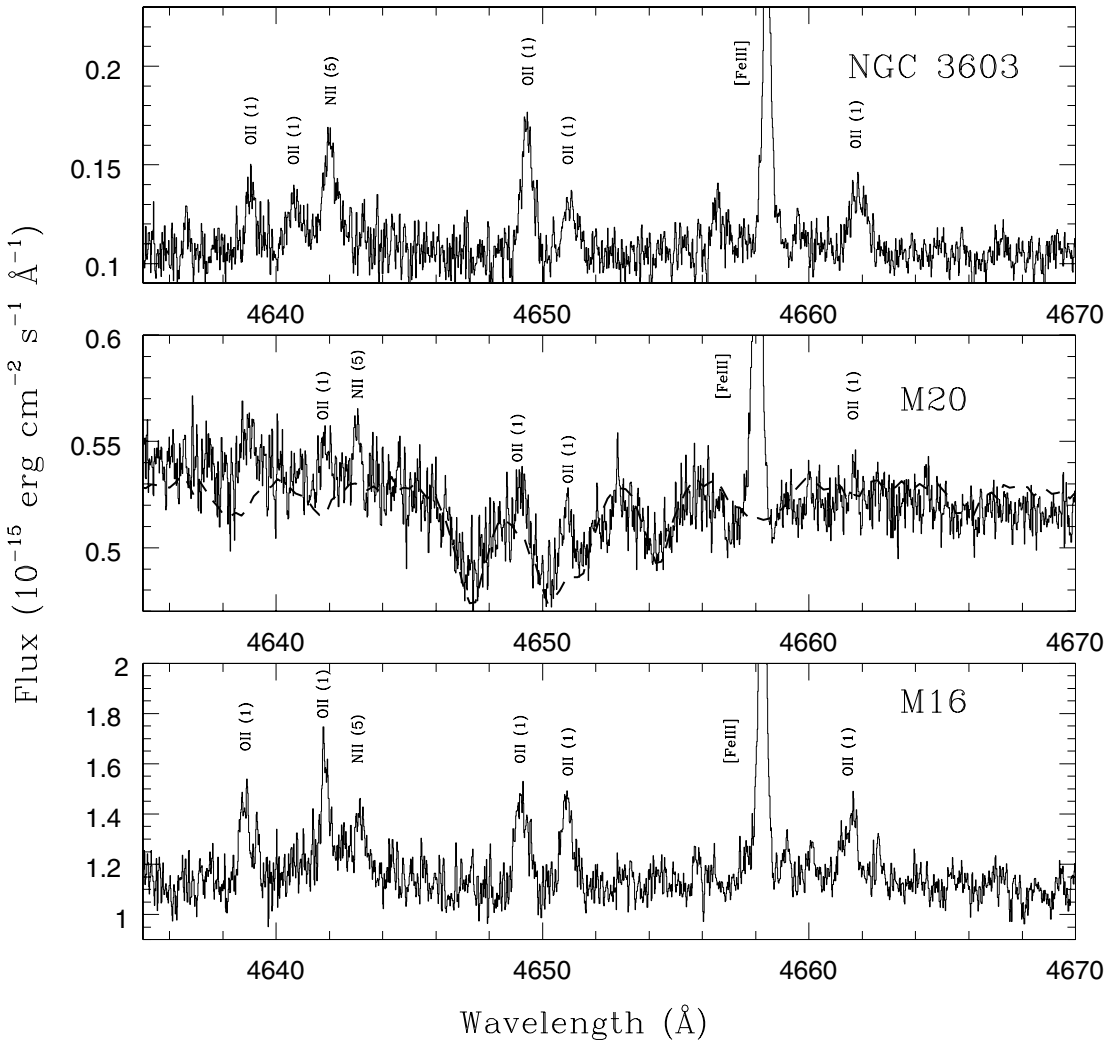

Figure 2. Section of the echelle spectra showing the lines of multiplet 1 of O II (observed fluxes) for the three H II regions. In the case of M20, we have superimposed the spectrum of HD164492 (dashed line), which is normalized to the continuum flux in the zone of O II 4649 and 4650 Å lines. It can be seen that the fluxes of multiplet 1 emission lines may be measured simply by integrating the line flux between the closest points of the local adjacent continuum, and that these lines are not seriously attenuated by the dust-scattered light (see text).

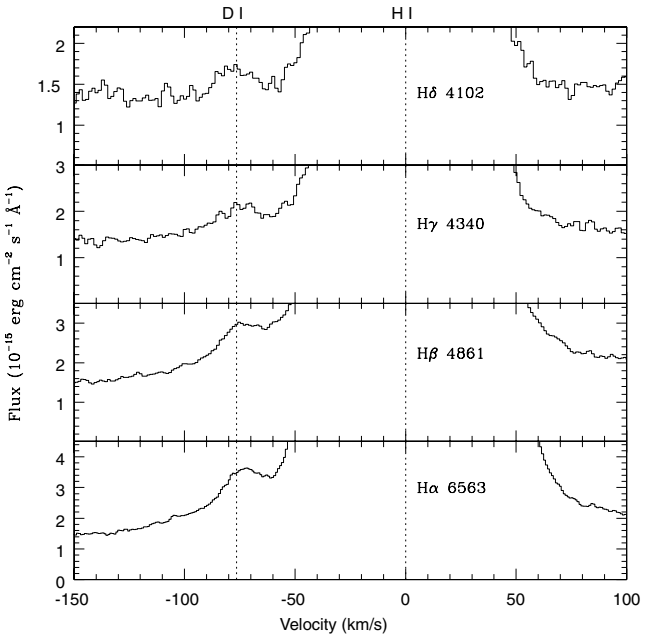

Figure 3. Wings of Hα to Hδ in M16. The lines are centred at 0 km s^{-1} velocity. The dotted line of the left-hand panel corresponds to the average wavelength adopted for the D I lines.

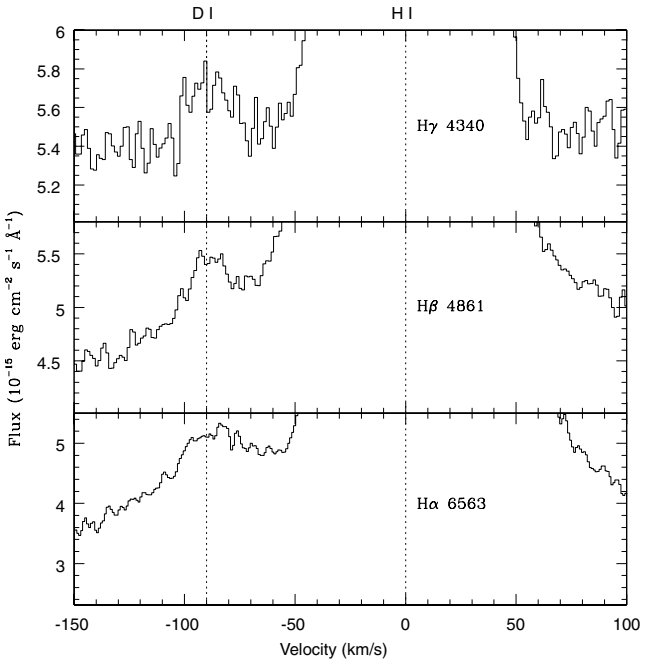

Figure 4. Same as Fig. 4 for M20.

is the absence of similar high-velocity components associated to bright lines of other ions. The second is that the FWHM of the deuterium lines is narrower than 10 km s^{-1} in all cases, much narrower than the H I Balmer lines (see Figs 3 and 4), which have FWHM between 20 and 25 km s^{-1}. This fact supports the idea that deuterium lines arise from much colder material, probably from the photon-dominated region (Hébrard et al. 2000).

In order to strengthen the conclusions about the nature of the emission of D I Balmer lines, we have compared the Balmer decrements of the hydrogen and deuterium lines observed in our spectra with the standard fluorescence models by O'Dell, Ferland & Henney (2001, see their fig. 13) for the Orion nebula, finding that our observations follow closely this model, indicating that fluorescence should be the main excitation mechanism of the D I lines observed in M16 and M20 (see Table 11).

Table 11. Deuterium Balmer line properties in M16 and M20.

Line	D I isotopic shift (km s^{-1})	FWHM D I (km s^{-1})	FWHM H I (km s^{-1})	D I/H I ratio ($\times 10^{-4}$)
M16				
α	−75.4	<10:	24	1.0 ± 0.3
β	−76.5	<10:	24	3.2 ± 0.9
γ	−76.7	<10:	24	6.4 ± 2.4
δ	−77.5	<10:	24	8.2:
M20				
α	−92.7	<10:	25	2.0 ± 0.4
β	−90.7	<10:	20	3.9 ± 1.5
γ	−89.1	<10:	21	4.7:

8 HIGH-VELOCITY COMPONENTS IN NGC 3603

We have detected weak emission features in the red wing of the highest ionization potential lines in the spectrum of NGC 3603: those of [Ar IV] −40.74 eV, and [Cl IV] −39.61 eV (see Fig. 5). These features are redshifted ∼36 km s^{-1} (argon), and ∼33 km s^{-1} (chlorine) with respect to the [Ar IV] and [Cl IV] lines. The FWHM of these presumed high-velocity components is similar (∼18 km s^{-1}) to that of the main component. The redshifted component is also detectable in the line profiles of other lines (see Fig. 6), but it is much less evident, with a contrast that decreases as the ionization potential of the ion that produces the line decreases. This indicates that the redshifted component is composed of a gas with

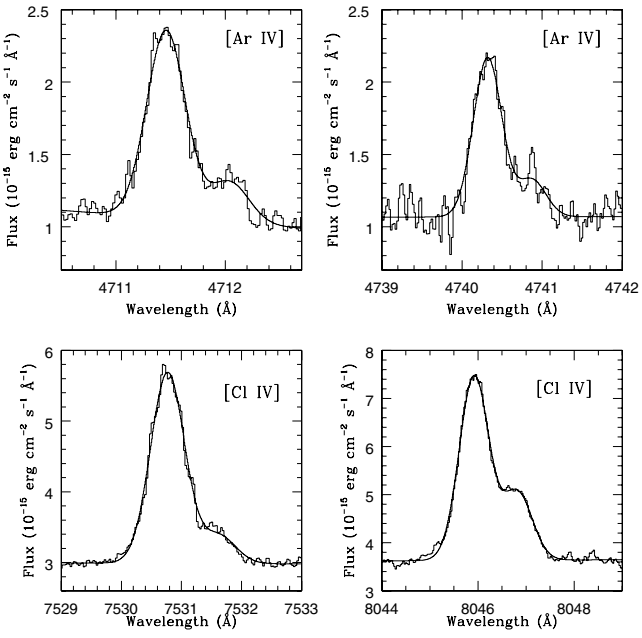

Figure 5. Redshifted components in the wings of [Ar IV] and [Cl IV] lines in NGC 3603.

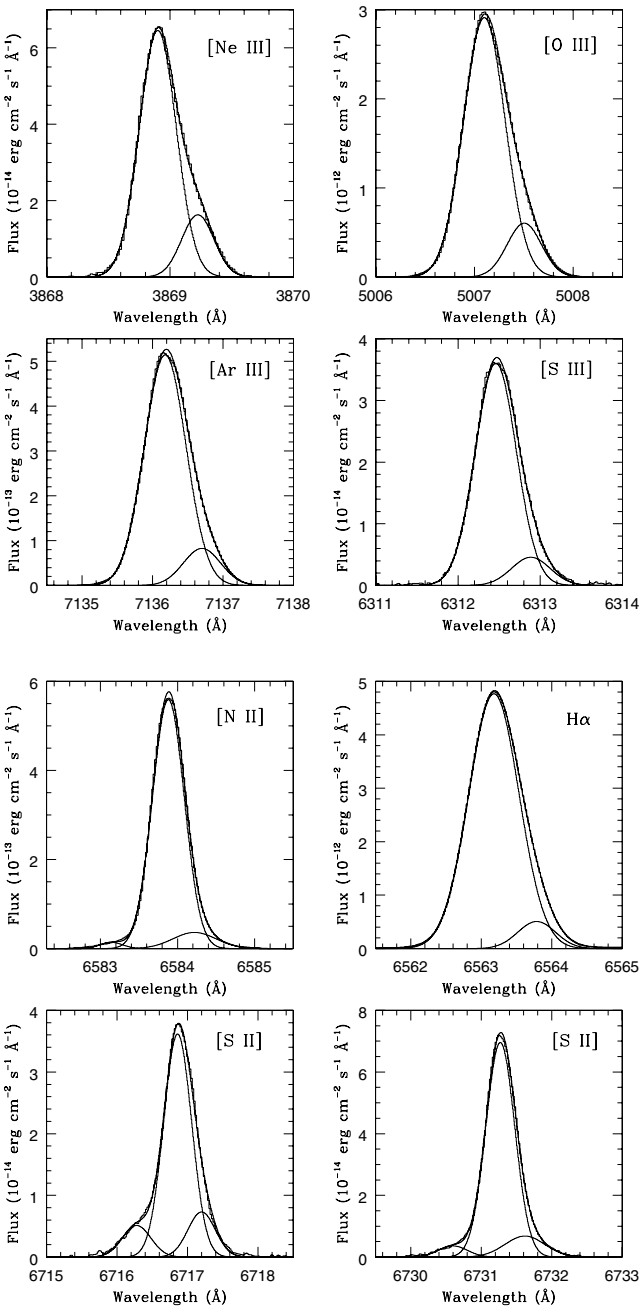

Figure 6. Components in the wings of [Ne III], [O III], [Ar III], [S III], [N II], [S II] lines and Hα in NGC 3603. Ionization potential of the ions that produce the lines decreases from top to bottom panel and from left-hand to right-hand panel.

a higher ionization degree than the main component. An additional fainter and blue-shifted component seems to be present in the lines of the low ionization potential ions, as [N II] and [S II].

Clayton (1990) obtained high spectral resolution [O III] profiles at different zones of NGC 3603, finding a clear red component in the [O III] 5007 Å line along most of the spatial extension of the nebula. At or very near our slit position, he detected that this second component shows a velocity shift between 30 and 40 km s^{-1}, with respect to the main one, values consistent with our reported velocity separations. The gas motions in NGC 3603 are rather complex and

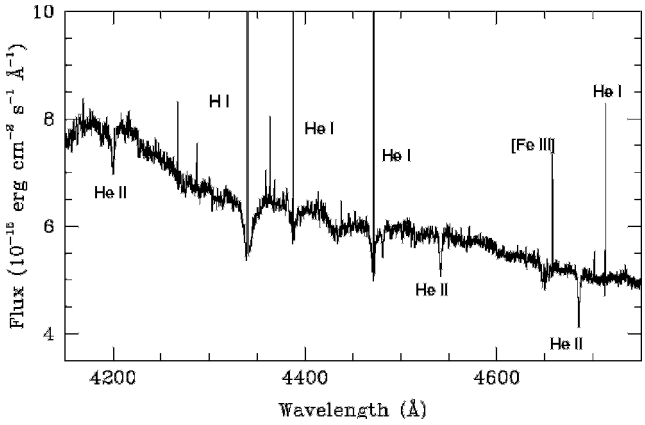

Figure 7. Section of the echelle spectrum showing the absorption λλ4200 Å, 4542 and 4686 Å He^+ lines.

can be interpreted as the product of different expanding structures with velocities up to 100 km s^{-1}.

9 DISCUSSION

In order to improve the clarity of this paper, we have divided the discussion in different subsections, one devoted to M16 and M20, and another one devoted to the discussion of NGC 3603, whose peculiarities and its status as a Galactic example of giant H II region make it a specially interesting object.

9.1 M20 and M16

9.1.1 M20 continuum determinations

In the case of M20, our slit position is located in a bright zone very near its ionizing star HD164492 (17 arcsec north and 10 arcsec east). This bright zone is just at the border of one of the dust lanes that crosses the nebula. Therefore, it is not strange that the stellar scattered light contribution in these spectra is specially high. This can be noted in the absorption features present in Figs 2 and 7, where we detect the stellar He II absorptions at λλ4200, 4542 and 4686 Å as well as absorption in the H I Balmer lines.

In Table 12, we show the observed and the expected nebular continua as well as the estimated scattered light contribution for different wavelengths. The nebular atomic continuum is the sum of the continua produced by H I and He I and it has been derived for the physical conditions and the He/H ratio computed for M20. From the table, it is evident that the scattered light is the main contribution to the observed continuum. As expected for normal dust properties, we

Table 12. M20 Continuum determinations.[a]

λ(Å)	log [j(λ)/j(Hβ)]		
	Atomic	Observed	Scattered light
3640	−2.179	−1.528 ± 0.007	−1.638 ± 0.008
3670	−3.094	−1.634 ± 0.004	−1.649 ± 0.004
4110	−3.246	−1.733 ± 0.003	−1.746 ± 0.003
4350	−3.281	−1.818 ± 0.004	−1.833 ± 0.004
4850	−3.316	−2.007 ± 0.004	−2.029 ± 0.004
6570	−3.346	−2.370 ± 0.006	−2.419 ± 0.008
8175	−3.332	−2.674 ± 0.002	−2.783 ± 0.003
8260	−4.001	−2.678 ± 0.008	−2.957 ± 0.015

[a]In units of (Å^{-1}).

have also found that the amount of stellar scattered light increases systematically towards bluer wavelengths (see Table 12). Using the observed equivalent widths of the He II absorption lines and those detected in the spectrum of HD164492,[3] it is possible to estimate the fraction of dust scattered light, using the expression used by Sánchez & Peimbert (1991):

$$\frac{i_{\rm d}(\lambda)}{i} = \frac{\sum \mathrm{EW(M20)}}{\sum \mathrm{EW(HD164492)}}, \quad (4)$$

where $i_{\rm d}(\lambda)/i$ is the fraction of dust scattered light in M20 with respect to the total emission of HD164492 at a given wavelength range. From this expression, we have obtained $i_{\rm d}/i = 0.54 \pm 0.09$; on the other hand, the fraction of the continuum scattered light with respect to the observed continuum in the 4200–4850 Å range in M20 amounts to 0.96 ± 0.01. O'Dell, Hubbard & Peimbert (1966) reported that the effective dust-to-gas ratio is five times higher in M20 than in other gaseous nebulae or the interstellar medium; also, Robledo-Rella (2002) reported that the nebular continuum of M20 is strongly dominated by dust-scattered light. These results agree with the high fraction of dust scattered light observed in the continuum of M20. This high fraction of dust scattered light could be due to the closeness of our slit position to HD164492; moreover, other nearby stars could be contributing to the observed continuum.

9.1.2 Comparison with other abundance determinations

As we have stated in Section 5.2, we have derived our ionic abundances from CELs making use of all the individual lines (which are not blended with other lines) of each ion observed. All the individual ionic abundances are consistent, within the errors, with the adopted weighted mean, except for the case of S^+, for which we have obtained larger differences because we have used $T_{\rm e}$(low) instead of $T_{\rm e}$([S II]) to derive S^+ abundances. In fact, the largest differences are between abundances derived from λλ 6717, 6731 Å and from λλ 10329, 10336 and 10371 Å, (over 0.15 dex in the case of M16), but these last lines have less weight in the final adopted value.

Previous abundance determinations in M20 and M16 are those of Hawley (1978) and Rodríguez (1998, 1999b). All of them are based on the analysis of CELs. Although the slit positions studied in these works are different, we have compared their results with ours. For the sake of consistency, we have re-computed the abundances given by those authors using the same set of atomic data and ICF scheme than in this paper. Moreover, taking into account that the previous works obtained abundances in several slit positions across the nebula, we have taken average values for the comparison.

In general, there is a good agreement between our O, N and S abundances obtained from CELs and those obtained by Hawley (1978) within the errors. Departures from our values are smaller than 0.1 dex for N, and the O abundance is almost coincident in the case of M20 and 0.09 dex lower in the case of M16. Taking into account that Hawley highlighted the difficulties in the measurement of some lines (those of [N II] and [S III]) in his spectra, the agreement with our results is remarkable.

We have followed the same methodology to compare with the results of Rodríguez (1998, 1999b). For M20, N and S show differences of 0.06 and 0.09 dex, respectively, but the O abundance shows a larger discrepancy (0.21 dex), mainly due to the differences in the O^+/H^+ ratio. This difference can be explained because Rodríguez determined the O^+/H^+ ratio from the [O II] 7320+7330 Å lines, which were severely affected by sky telluric lines (Rodríguez 1998). For M16, there is a good agreement between our results and Rodríguez ones, specially for N and S abundances, which are almost coincident with our values. The discrepancy in the O abundance is, in this case, of 0.11 dex, probably due to the same reason pointed out above.

9.2 NGC 3603

As it was commented in Introduction, NGC 3603 is the only Galactic giant H II region that can be observed in the visual. Melnick et al. (1989) derived an O abundance for NGC 3603 of $12 + \log(\mathrm{O/H}) = 8.39 \pm 0.41$. In spite of its extremely large uncertainty, this value is in good agreement with our derived O/H abundance ratio from CELs. On the other hand, Tapia et al. (2001) published the most complete set of abundances in the literature for NGC 3603 until now; their O/H ratio is only 0.06 dex higher than ours, and the large differences in the other abundance ratios are probably due to their large line-intensity uncertainties and the different set of ICFs used. We have found a similar behaviour, comparing our abundances based on CELs with those of Girardi et al. (1997).

For NGC 3603, we have available O, N, Ne and S abundance determinations based on far-infrared fine-structure line observations (Simpson et al. 1995). Since the emissivity of these lines is essentially independent of the nebular thermal structure – due to their low excitation energies, it is interesting to compare abundances derived from these lines with those derived from RLs or from optical CELs assuming a t^2. In principle, assuming the temperature fluctuation paradigm, and that there are no large density fluctuations, all these determinations might be similar. In Table 13, we compare our derived total and ionic abundances for NGC 3603 (this work) with those obtained by Simpson et al. (1995). In spite of the high uncertainty of the abundances derived by Simpson et al. (1995) (due to the uncertainty in the radio flux and aperture effects), values derived from infrared (IR) CELs and those derived from optical CELs assuming a $t^2 > 0$ are similar, a fact that seems to support the presence of temperature fluctuations in the nebula. However, there are other examples where this is not clear; from a similar comparison between optical data and Simpson's IR data, other results have been found: NGC 3576 (Tsamis et al. 2003; García-Rojas et al. 2005) and Orion nebula (Tsamis et al. 2003; Esteban et al. 2004) shows IR abundances which are intermediate between $t^2 = 0.00$ and $t^2 > 0$, and M17 (Esteban et al. 1999a; Tsamis et al. 2003) and 30 Doradus (Peimbert 2003; Tsamis et al. 2003) shows IR abundances which are rather similar to those derived from optical CELs and $t^2 = 0.00$. Moreover, the comparison of our slit optical spectroscopy and the

Table 13. Comparison of optical and IR abundances for NGC 3603.[a]

Element/ion	Optical CELs[b] ($t^2 = 0.00$)	Optical CELs[b] ($t^2 > 0.00$)	IR CELs[c]
O	8.46 ± 0.05	8.72 ± 0.05	8.79 ± 0.09
N	7.62 ± 0.13	7.89 ± 0.14	7.96 ± 0.09
S	7.03 ± 0.05	7.36 ± 0.08	7.12 ± 0.09
Ne	7.76 ± 0.08	8.03 ± 0.11	8.08
O^{++}	8.42 ± 0.05	8.68 ± 0.08	8.61 ± 0.09
S^{++}	6.83 ± 0.04	7.11 ± 0.09	6.90 ± 0.12
Ne^{++}	7.72 ± 0.05	8.00 ± 0.08	7.85 ± 0.09

[a]In logarithmic units. [b]This work. [c]Simpson et al. (1995).

[3] This spectrum was obtained with the Intermediate Dispersion Spectrograph (IDS) attached to the INT 2.5-m Telescope of the Roque de los Muchachos Observatory in La Palma, Spain. The results used here were kindly provided by Sergio Simón-Díaz (private communication).

IR data of Simpson et al. (1995) shows a further complication, at least for the ionic abundances. The aperture used in both kinds of observations covers a very different area of the nebula, which is much larger in the IR spectroscopy. Changes in the mean ionization degree of the area covered in optical and IR observations may produce natural differences in the ionic abundances not related to the presence or absence of a temperature structure. In contrast, this effect should not affect the total abundances. In this sense, we think important to clarify the conclusion drawn by Tsamis et al. (2003) about this issue. Those authors make the comparison between the O^{++}/H^{+} abundances derived from optical and IR CELs for a sample of H II regions, and conclude that temperature fluctuations might be ruled out as the cause of the discrepancy found between O^{++}/H^{+} abundances derived from optical RLs and CELs. From our apparently positive results for NGC 3603 and taking into account the aperture consideration, that conclusion seems to be far from conclusive. It is clear that further IR and optical observations taken in the same zones and with similar apertures are needed to settle definitively this problem.

10 CONCLUSIONS

We present deep echelle spectroscopy in the 3100–10 400 Å range of bright zones of the Galactic H II regions: M16, M20 and NGC 3603. We have measured the intensity of about 250 lines per object. This is the most complete set of emission lines ever obtained for these three objects.

We have derived the physical conditions of each nebula, making use of several line intensities and continuum ratios. The chemical abundances have been derived using the intensity of CELs for a large number of ions of different elements. We have determined, for the first time in the three objects, the C^{++} and O^{++} abundances from RLs and, finally, we have also determined the abundance of O^{+} from RLs for the first time in M20.

We have obtained consistent estimations of the temperature fluctuations parameter, t^2, applying different methods: by comparing the O^{+} (when available) and O^{++} ionic abundances derived from RLs to those derived from CELs; by applying a chi-squared method which minimizes the dispersion of He^{+}/H^{+} ratios from individual lines; and by comparing the electron temperatures derived from CELs to those derived from Balmer and Paschen continua. The adopted average value of t^2 has been used to correct the ionic abundances derived from CELs.

We report the detection of several deuterium Balmer lines in the spectra of M16 and M20. The properties of these lines indicate that fluorescence is their most probable excitation mechanism.

We have compared the results obtained for optical CELs in NGC 3603 with those obtained from far-infrared fine-structure CELs, finding an apparent agreement, in spite of the high uncertainties of the abundances derived from far-infrared data, if the temperature fluctuation paradigm is assumed. However, IR and optical spectrophotometry covering the same volume of the nebula is necessary to make a reliable and conclusive comparison between optical and IR CEL abundances.

ACKNOWLEDGMENTS

This work is based on observations collected at the European Southern Observatory, Chile, proposal number ESO 68.C-0149(A). We want to thank an anonymous referee for his/her comments that have increased the quality of this work. JG-R and CE would like to thank the members of the Instituto de Astronomía, UNAM, and of the INAOE, Puebla for their ever-warm hospitality. JGR would like to thank S. Simón-Díaz and A. R. López-Sánchez for fruitful discussions. This work has been partially funded by the Spanish Ministerio de Ciencia y Tecnología (MCyT) under projects AYA2001-0436 and AYA2004-07466. MP received partial support from DGAPA UNAM (grant IN 114601). MTR received partial support from FONDAP(15010003) and Fondecyt(1010404). MR acknowledges support from Mexican CONACYT project J37680-E.

REFERENCES

Balick B., Boeshaar G. O., Gull T. R., 1980, ApJ, 242, 584
Bautista M. A., Pradhan A. K., 1996, A&AS, 115, 551
Benjamin R. A., Skillman E. D., Smits D. P., 1999, ApJ, 514, 307
Benjamin R. A., Skillman E. D., Smits D. P., 2002, ApJ, 569, 288
Bohlin R. C., Lindler D., 1992, STScI Newslett. Vol. 9, 2, 19
Bohuski T. J., 1973a, ApJ, 183, 851
Bohuski T. J., 1973b, ApJ, 184, 93
Brandl B., Brandner W., Eisenhauer F., Moffat A. F. J., Palla F., Zinnecker H., 1999, A&A, 352, L69
Brown R. L., Mathews W. G., 1970, ApJ, 160, 939
Cardelli J. A., Clayton G. C., Mathis J. S., 1989, ApJ, 345, 245
Caswell J. L., Haynes R. F., 1987, A&A, 171, 261
Chini R., Wargau W. F., 1990, A&A, 227, 213
Clayton C. A., 1986, MNRAS, 219, 895
Clayton C. A., 1990, MNRAS, 246, 712
Copetti M. V. F., Mallmann J. A. H., Schmidt A. A., Castañeda H. O., 2000, A&A, 357, 621
Deharveng L., Peña M., Caplan J., Costero R., 2000, MNRAS, 311, 329
D'Odorico S., Cristiani S., Dekker H., Hill V., Kaufer A., Kim T., Primas F., 2000, in Bergeron J., ed., Proc. SPIE, Vol. 4005, Discoveries and Research Prospects from 8- to 10-Meter-Class Telescopes. SPIE, Bellingham WA, p. 121
Dopita M. A., 1974, A&A, 32, 121
Escalante V., Victor G. A., 1992, Planet. Space Sci., 40, 1705
Esteban C., 2002, Rev. Mexicana Astron. Astrofis. Conf. Ser., 12, 56
Esteban C., Peimbert M., Torres-Peimbert S., Escalante V., 1998, MNRAS, 295, 401
Esteban C., Peimbert M., Torres-Peimbert S., García-Rojas J., 1999a, Rev. Mexicana Astron. Astrofis., 35, 65
Esteban C., Peimbert M., Torres-Peimbert S., García-Rojas J., Rodríguez M., 1999b, ApJS, 120, 113
Esteban C., Peimbert M., Torres-Peimbert S., Rodríguez M., 2002, ApJ, 581, 241
Esteban C., Peimbert M., García-Rojas J., Ruiz M. T., Peimbert A., Rodríguez M., 2004, MNRAS, 355, 229
Esteban C., García-Rojas J., Peimbert M., Peimbert A., Ruiz M. T., Rodríguez M., Carigi L., 2005, ApJ, 618, L95
García-Rojas J., Esteban C., Peimbert A., Peimbert M., Rodríguez M., Ruiz M. T., 2005, MNRAS, 362, 301
García-Rojas J., Esteban C., Peimbert M., Rodríguez M., Ruiz M. T., Peimbert A., 2004, ApJS, 153, 501
Girardi L., Bica E., Pastoriza M. G., Winge C., 1997, ApJ, 486, 847
Goss W. M., Radhakrishnan V., 1969, Astrophys. Lett., 4, 199
Grandi S. A., 1976, ApJ, 206, 658
Hamuy M., Walker A. R., Suntzeff N. B., Gigoux P., Heathcote S. R., Phillips M. M., 1992, PASP, 104, 533
Hamuy M., Suntzeff N. B., Heathcote S. R., Walker A. R., Gigoux P., Phillips M. M., 1994, PASP, 106, 566
Hawley S. A., 1978, ApJ, 224, 417
Hébrard G., Péquignot D., Walsh J. R., Vidal-Madjar A., Ferlet R., 2000, A&A, 364, L31
Hester J. J. et al., 1996, AJ, 111, 2349
Howard I. D., Murray J., 1990, SERC Starlink User Note No. 50
Kingdon J., Ferland G. J., 1995, ApJ, 442, 714
Krishna Swamy K. S., O'Dell C. R., 1967, ApJ, 147, 529
Lacy J. H., Beck S. C., Geballe T. R., 1982, ApJ, 255, 510

Liu X.-W., Storey P. J., Barlow M. J., Danziger I. J., Cohen M., Bryce M., 2000, MNRAS, 312, 585
Liu X.-W., Luo S.-G., Barlow M. J., Danziger I. J., Storey P. J., 2001, MNRAS, 327, 141
Lynds B. T., O'Neil E. J., 1985, ApJ, 294, 578
McCaughrean M. J., Andersen M., 2002, A&A, 389, 513
Melnick J., Tapia M., Terlevich R., 1989, A&A, 213, 89
Nürnberger D. E. A., Bronfman L., Yorke H. W., Zinnecker H., 2002, A&A, 394, 253
O'Dell C. R., Hubbard W. B., Peimbert M., 1966, ApJ, 143, 743
O'Dell C. R., Ferland G. J., Henney W. J., 2001, ApJ, 556, 203
Peimbert A., 2003, ApJ, 584, 735
Peimbert M., 1967, ApJ, 150, 825
Peimbert M., 1971, Boletin de los Observatorios Tonantzintla y Tacubaya, 6, 29
Peimbert M., Costero R., 1969, Boletin de los Observatorios Tonantzintla y Tacubaya, 5, 3
Peimbert M., Torres-Peimbert S., 1977, MNRAS, 179, 217
Peimbert M., Torres-Peimbert S., Ruiz M. T., 1992, Rev. Mexicana Astron. Astrofis., 24, 155
Peimbert M., Storey P. J., Torres-Peimbert S., 1993, ApJ, 414, 626
Peimbert M., Peimbert A., Ruiz M. T., 2000, ApJ, 541, 688
Peimbert A., Peimbert M., Luridiana V., 2002, ApJ, 565, 668
Peimbert A., Peimbert M., Ruiz M. T., 2005, ApJ, 634, 1056
Pequignot D., Petitjean P., Boisson C., 1991, A&A, 251, 680
Quinet P., 1996, A&AS, 116, 573
Reifenstein E. C., Wilson T. L., Burke B. F., Mezger P. G., Altenhoff W. J., 1970, A&A, 4, 357
Robledo-Rella V., 2002, Rev. Mexicana Astron. Astrofis. Conf. Ser., 12, 31
Rodríguez M., 1996, A&A, 313, L5
Rodríguez M., 1998, PhD thesis, La Laguna University
Rodríguez M., 1999a, A&A, 348, 222
Rodríguez M., 1999b, A&A, 351, 1075
Rodríguez M., 2002, A&A, 389, 556
Rodríguez M., Rubin R. H., 2005, ApJ, 626, 900
Rosado M., Esteban C., Lefloch B., Cernicharo J., García López R. J., 1999, AJ, 118, 2962
Ruiz M. T., Peimbert A., Peimbert M., Esteban C., 2003, ApJ, 595, 247
Sánchez L. J., Peimbert M., 1991, Rev. Mexicana Astron. Astrofis., 22, 285
Savage B. D., Mathis J. S., 1979, ARA&A, 17, 73
Sawey P. M. J., Berrington K. A., 1993, Atomic Data and Nuclear Data Tables, 55, 81
Seaton M. J., 1979, MNRAS, 187, 73P
Shaver P. A., Goss W. M., 1970, Aust. J. Phys. Astrophys. Supp., 14, 133
Shaw R. A., Dufour R. J., 1995, PASP, 107, 896
Simpson J. P., Colgan S. W. J., Rubin R. H., Erickson E. F., Haas M. R., 1995, ApJ, 444, 721
Smits D. P., 1996, MNRAS, 278, 683
Stolte A., Brandner W., Brandl B., Zinnecker H., Grebel E. K., 2004, AJ, 128, 765
Storey P. J., Hummer D. G., 1995, MNRAS, 272, 41
Tapia M., Bohigas J., Pérez B., Roth M., Ruiz M. T., 2001, Rev. Mexicana Astron. Astrofis., 37, 39
Thompson R. I., Smith B. A., Hester J. J., 2002, ApJ, 570, 749
Torres-Peimbert S., Peimbert M., 1977, Rev. Mexicana Astron. Astrofis., 2, 181
Torres-Peimbert S., Peimbert M., Daltabuit E., 1980, ApJ, 238, 133
Tsamis Y. G., Barlow M. J., Liu X.-W., Danziger I. J., Storey P. J., 2003, MNRAS, 338, 687
Tsamis Y. G., Barlow M. J., Liu X.-W., Storey P. J., Danziger I. J., 2004, MNRAS, 353, 953
Tsamis Y. G., Péquignot D., 2005, MNRAS, 364, 687
Turnshek D. A., Bohlin R. C., Williamson R. L., Lupie O. L., Koornneef J., Morgan D. H., 1990, AJ, 99, 1243
Verner E. M., Verner D. A., Baldwin J. A., Ferland G. J., Martin P. G., 2000, ApJ, 543, 831
Zhang H., 1996, A&AS, 119, 523

This paper has been typeset from a TEX/LATEX file prepared by the author.